Geophys. J. Int. (2003) **154,** 783–800

Two-dimensional convection with a self-lubricating, simple-damage rheology

Christian Auth,[1,2] David Bercovici[2,*] and Ulrich R. Christensen[1,†]

[1] *Universität Göttingen, Institut für Geophysik, Herzberger Landstr.* 180, 37075 *Göttingen, Germany*
[2] *University of Hawaii, Department of Geology and Geophysics, SOEST,* 1680 *East West Road, Honolulu* HI 96822, *USA*

Accepted 2003 March 20. Received 2003 February 14; in original form 2002 January 21

SUMMARY

We present 2-D simulations of convection in the Earth's mantle with temperature and damage-dependent viscosity in a basally heated system. The equation governing the temporal evolution of damage includes a source term for damage, a healing term and an advection term. A systematic study of the influence of the different damage terms on the convection pattern shows that: (1) at least four different convective regimes can be distinguished depending on the size of the damage source term and (2) self-lubricating behaviour is possible only if the advection term in the damage equation is small enough compared with the other terms. We also demonstrate, that good plate-like behaviour in terms of (a) focused low-viscosity bands (LVB), (b) homogeneous surface velocities within the plates and abrupt velocity jumps across the plate boundaries and (c) asymmetric subduction, can be obtained with this kind of rheology, although an increase in subduction asymmetry tends to make convection highly time-dependent.

Key words: lithospheric deformation, mantle convection, plate tectonics.

1 INTRODUCTION

Understanding the driving mechanisms associated with the motions of the Earth's major tectonic plates remains one of the fundamental questions in geophysics. Many mantle convection models have been developed to explain the basic principles of terrestrial plate tectonics, however, computer simulations usually have problems reproducing important observed features such as the concentration of deformation at plate boundaries, the existence of continuous asymmetric subduction zones, or the poloidal:toroidal (i.e. divergent versus strike-slip) energy ratios. For a discussion of plate-like behaviour in mantle convection models we refer to recent reviews (Bercovici *et al.* 2000; Tackley 2000a,d; Bercovici 2003). Here we will address only a few very recent studies, which we sort into two groups. The first group consist of calculations that incorporate pseudo-plastic yield-stress rheologies into the hydrodynamic equations. Trompert & Hansen (1998) reported that this kind of rheology can lead to highly episodic subduction behaviour, including homogeneous (i.e. solid-body or plate-like) surface velocities and asymmetric subduction during the 'active' episodes. However, convection in their model seems to be more Venus- than Earth-like, since all cold and high-viscosity material of a subducting plate rapidly vanishes into the deep mantle and the lithosphere has to redevelop during the 'passive' periods of the system. Using a similar rheology, Tackley (2000b) found by varying the yield stress, that first-order plate-like behaviour can be obtained only in 'a narrow range of yield strength, below which diffuse boundaries, and above which episodic behaviour and eventually a rigid lid are observed'. The introduction of a low-viscosity asthenosphere and melting improved those results significantly (Tackley 2000c). Models in the second group use rheologies with the possibility for self-lubrication. A self-lubricating rheology has a stress (σ) versus strain rate ($\dot{\varepsilon}$) curve, which is not monotonically increasing, but has a maximum stress ($\sigma_{\max}$) and a negative slope for $\dot{\varepsilon} > \dot{\varepsilon}_{\max}$ (Bercovici 1993, 1995; Tackley 1998). Bercovici (1998) used a model, in which the viscosity depends on an additional 'damage' parameter (in Bercovici's paper the porosity of the material), for which the temporal evolution is described by a separate conservation equation. In the limit of a negligible advection term in this conservation equation, we obtain a self-lubricating rheology (see below). Bercovici was able to show, that highly focused transform faults in a 2-D horizontal layer can be obtained with this model. Tackley (2000c) later added Bercovici's rheology to his model (see above), but concluded that it has too much of a damaging effect on oceanic plate dynamics, causing excessive breakdown of plates into small segments. However, another feature of Bercovici's rheology is, that it is not 'instantaneous', but 'history dependent'. Because of the time dependence of the damage parameter, the material essentially 'remembers' its deformational history, which is important, since the existence of long-lived weak zones in the lithosphere is thought to influence plate tectonics (Gurnis *et al.* 2000). It should be noted, however, that these simple damage

*Now at: Yale University, Department of Geology and Geophysics, PO Box 208109, New Haven, CT 06520-8109, USA. E-mail: david.bercovici@yale.edu
†Now at: Max-Planck Institut für Aeronomie, Max-Planck-Straße 2, 37191 Katlenburg-Lindau, Germany.

theories are somewhat *ad hoc*; more sophisticated, first-principles-based (and consequently more complicated) damage theories for lithospheric shear-localization have been proposed more recently (Bercovici *et al.* 2001a,b; Ricard *et al.* 2001; Ricard & Bercovici 2003; Bercovici & Ricard 2003).

In this article, a rheology similar to Bercovici's is incorporated into a 2-D mantle convection model, to investigate the possibilities of this kind of rheology systematically. In contrast to Tackley's models, the damage parameter is the only parameter (except for the temperature) to influence the viscosity. Since an important aspect of our investigations will be to look for symmetry breaking in the convection pattern we will use bottom heating (the simplest symmetrical heating mode) in our models. Internal heating might be more Earth-like, but it imposes asymmetry between up- and downwellings.

2 THE MODEL

The basic equations in our model are the usual hydrodynamic equations for a bottom-heated system within the Boussinesq approximation and with infinite Prandtl number. We present them in the non-dimensional form used in Christensen & Harder (1991):

$$\boldsymbol{\nabla} \cdot \mathbf{u} = 0 \tag{1}$$

$$-\boldsymbol{\nabla} p + \boldsymbol{\nabla} \cdot (\eta \underline{\dot{\varepsilon}}) + RaT\hat{\mathbf{z}} = 0 \tag{2}$$

$$\frac{\partial T}{\partial t} + \mathbf{u} \cdot \boldsymbol{\nabla} T = \nabla^2 T. \tag{3}$$

Here $\mathbf{u} = (u_x, u_z)$ denotes the velocity vector, p the non-hydrostatic pressure, T the temperature, η the viscosity and $\underline{\dot{\varepsilon}}$ is the strain rate tensor defined as

$$\dot{\varepsilon}_{ij} = \frac{\partial u_i}{\partial x_j} + \frac{\partial u_j}{\partial x_i}. \tag{4}$$

The boundary conditions on the sidewalls are periodic; the upper and lower boundary are assumed to be impermeable, free slip and isothermal (i.e. $u_z = \partial^2 u_z / \partial\, z^2 = T + z - 1 = 0$ at $z = 0$, 1). The Rayleigh number for a bottom-heated system is defined as

$$Ra = \frac{\rho \alpha g \Delta T h^3}{\eta_0 \kappa}, \tag{5}$$

where α is the thermal expansivity, g is the gravitational acceleration, ΔT is the temperature drop over the box, h is the height of the box, κ is the thermal diffusivity, ρ is the density and η_0 is a dimensional reference viscosity (see below). The dimensionless viscosity η in our model depends on temperature T and an additional quantity d, termed the *damage parameter* (e.g. Lemaitre 1992; Krajcinovic 1996; Lyakhovsky *et al.* 1997; Bercovici 1998; Tackley 2000a; Bercovici *et al.* 2001a)

$$\eta = \frac{2}{1 + d^m} \mathrm{e}^{-\gamma T}, \tag{6}$$

where m and γ are input parameters. The reference viscosity η_0 used in the definition of Ra is thus the viscosity at $T = 0$ and $d = 1$.

The damage parameter d is assumed to be time dependent:

$$\frac{\partial d}{\partial t} + \mathbf{u} \cdot \boldsymbol{\nabla} d = a\sigma\dot{\varepsilon} - b\mathrm{e}^{\gamma T} d, \tag{7}$$

where $\dot{\varepsilon}$ and $\sigma = \eta\dot{\varepsilon}$ denote the second invariants of the strain-rate and stress tensors, defined as

$$\sigma = \left(\frac{1}{2} \sum_{i,j} \sigma_{ij}^2 \right)^{1/2}. \tag{8}$$

Eq. (7) is heuristic and its interpretation depends on what the damage parameter represents physically. Bercovici (1998) connects d to the porosity of the matrix mantle material, where the pores are assumed to be filled with a lower-viscosity fluid (see also Bercovici *et al.* 2001a; Ricard & Bercovici 2002; Bercovici & Ricard 2003).

His damage equation is somewhat similar to ours and a motivation for the sources and sinks of porosity is given in his 1998 paper. The interpretation for the damage our model is based on assumes d to be the inverse grain size of the material (Tackley 2000c). The viscosity law eq. (6) simply represents the harmonic average of a pure temperature-dependent viscosity $\eta_T = \mathrm{e}^{-\gamma T}$ and a grain-size dependent viscosity (diffusion creep) $\eta_\mathrm{d} = d^{-m}\mathrm{e}^{-\gamma T}$. The form of the sink term in eq. (7) is taken from investigations by Karato (1983) on grain growth except it assumes a linear d dependence. The input parameter b is the decay rate of d at $T = 0$. The source term $a\sigma\dot{\varepsilon}$ represents grain size reduction by dynamical recrystallization. Although a simple dependence on the strain rate and the inverse of the damage d (Braun *et al.* 1999) may be more obvious, we choose the form of eq. (7) to make our results more comparable to those of Tackley or Bercovici. What is important is not the exact form of eqs (6) and (7), but that they are physically plausible and, moreover, that they describe a rheology with the potential for self-lubricating mechanisms. We will show in the next section that our rheology has this potential.

3 BASIC EFFECTS OF THE DAMAGE RHEOLOGY

In this section, we discuss several aspects of our damage rheology in more detail. Our first point is to show that this rheology has the possibility for self-lubricating behaviour and for focused zones of high strain and low viscosity. This part follows calculations performed for similar rheologies by Bercovici (1996, 1998) and Tackley (1998). We also note that the frequently used term 'low-viscosity band' describes a region with a significant viscosity reduction compared with the corresponding pure temperature-dependent rheology, e.g. regions bearing significant damage.

3.1 Simple analysis without advection

If we neglect the advection term in eq. (7) and assume that the system will reach a steady state, we can then derive d as a function of $\dot{\varepsilon}$ by combining eqs (6) and (7) to obtain

$$d(1 + d^m) = 2\frac{a}{b}\eta_T^2 \dot{\varepsilon}^2, \tag{9}$$

where we recall that $\eta_T = \mathrm{e}^{-\gamma T}$. The solution $d(\dot{\varepsilon})$ to this equation can be substituted into eq. (6), and using $\sigma = \eta\dot{\varepsilon}$, we can write an effective constitutive law for stress σ as a function of strain rate $\dot{\varepsilon}$. For $m < 1$, the $\sigma(\dot{\varepsilon})$ curve is similar to power-law rheologies with a finite positive power-law exponent. The case for $m = 1$ represents a yield stress rheology, as used for example by Trompert & Hansen (1998); in this case the strain rate dependence of the stress can be determined analytically:

$$\sigma = \frac{4\eta_T \dot{\varepsilon}}{1 + \left[1 + 4(2a/b)\eta_T^2 \dot{\varepsilon}^2\right]^{1/2}}, \tag{10}$$

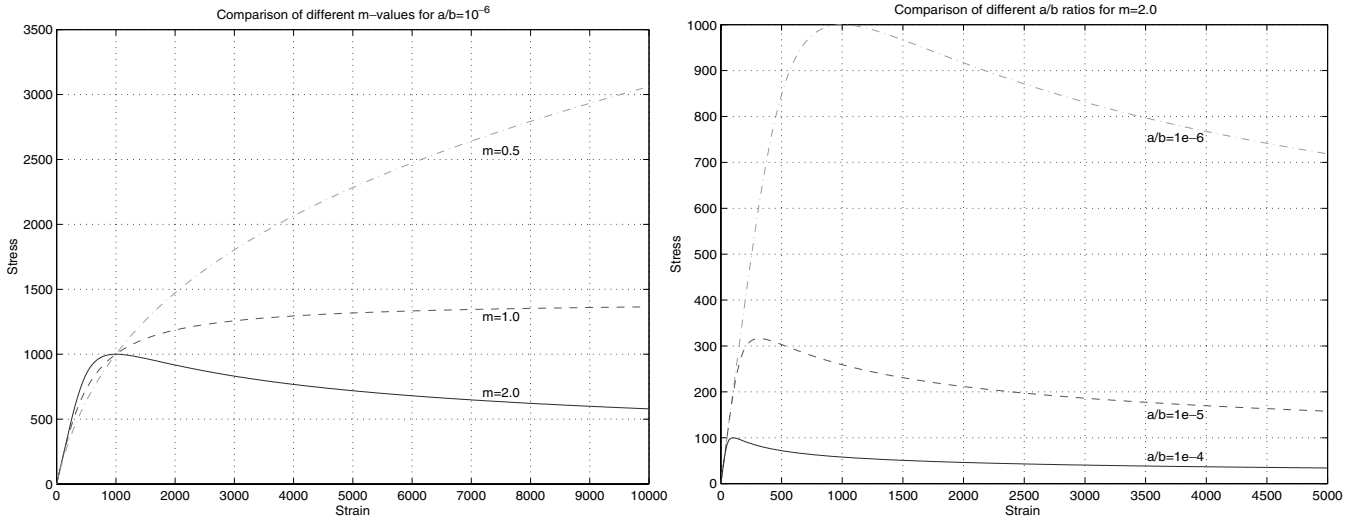

Figure 1. $\sigma(\dot{\varepsilon})$ curves in the limit of a vanishing advection term in the damage equation. Left: $\sigma(\dot{\varepsilon})$ for $m = 0.5$, $m = 1.0$ and $m = 2.0$ with $a/b = 10^{-6}$ fixed. Right: $\sigma(\dot{\varepsilon})$ for $m = 2.0$ fixed and $a/b = 10^{-4}$, $a/b = 10^{-5}$, $a/b = 10^{-6}$.

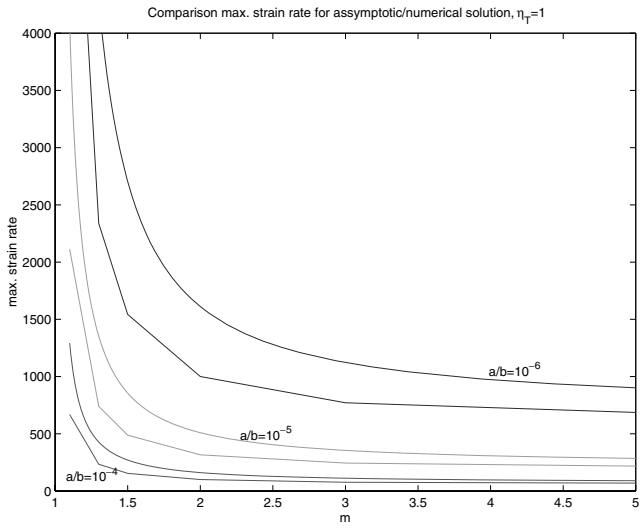

Figure 2. Maximum strain rate value versus m for our rheology in the limit of a vanishing advection term in the damage equation. Three different values from a/b are assumed. The smooth curves are approximations obtained from eq. (12), the others represent the exact values for selected m.

where, again, $\eta_T = \mathrm{e}^{-\gamma T}$. As $\dot{\varepsilon} \to \infty$ we obtain the yield stress $\sigma_{\mathrm{yield}} = (2\ b/a)^{1/2}$. For $m > 1$ all curves have a negative slope for strain rates larger than a special value $\dot{\varepsilon}_{\max}$; this is often referred to as a self-lubricating rheology (Bercovici 1996; 1998). Fig. 1 shows examples of $\sigma(\dot{\varepsilon})$ for typical values of the ratio a/b and different m. The parameter γ is assumed to be zero. Self-lubricating rheologies are difficult to handle in numerical simulations, because they tend to produce infinitesimally narrow shear zones with zero viscosities and discontinuous material velocities if the strain rate exceeds $\dot{\varepsilon}_{\max}$. Nevertheless, the low-viscosity bands in this model have to be properly resolved.

Fig. 2 shows the strain rate $\dot{\varepsilon}_{\max}$ for which the stress becomes maximal ($\sigma_{\max}$) as a function of the parameter m for different values of a/b. It can be seen that $\dot{\varepsilon}_{\max}$ is high for m close to unity and a/b small, but decreases for increasing m or a/b. To better understand this behaviour, we derive an analytical approximation of $\sigma(\dot{\varepsilon})$ for all m. Using eq. (9) and assuming $d \gg 1$ (such that $\eta = d^{-m}\eta_T$), we can solve for d for any value of m (we will, however, use the general expression $\eta = (1 + d^m)^{-1}\eta_T$ later; see below). It can be shown that these assumptions will give a good approximate solution for $\dot{\varepsilon} \ll 1$ and $\dot{\varepsilon} \gg 1$, and a reasonable form of the function $\dot{\varepsilon}_{\max}(a, b, m, \gamma)$ otherwise. We thus obtain

$$\sigma(\dot{\varepsilon}) = \frac{2\eta_T \dot{\varepsilon}}{1 + \left(2\frac{a}{b}\eta_T^2 \dot{\varepsilon}^2\right)^{m/(m+1)}} \tag{11}$$

leading to

$$\dot{\varepsilon}_{\max} = \left(\frac{b}{2a}\right)^{1/2} \left(\frac{1}{\eta_T}\right) \left(\frac{m+1}{m-1}\right)^{(m+1)/2m} \tag{12}$$

and

$$\sigma_{\max} = \left(\frac{2b}{a}\right)^{1/2} \left(\frac{m-1}{2m}\right) \left(\frac{m+1}{m-1}\right)^{(m+1)/2m}. \tag{13}$$

From eq. (11) it can be seen that, for $m < 1$, $\sigma(\dot{\varepsilon})$ is monotonically increasing. A maximum value $\sigma_{\max}$ is only obtained for $m \geq 1$. The decrease of $\dot{\varepsilon}_{\max}$ with increasing m is shown in eq. (12). It can also be seen from eqs (11) and (12), that for $m \to \infty$ a limiting value for $\dot{\varepsilon}_{\max}$ is reached. Moreover, $\dot{\varepsilon}_{\max}$ also depends on the ratio a/b. The general trend of this dependence is quite easy to understand: for $m > 1.0$ we obtain self-lubricating behaviour only if the viscosity in eq. (6) is significantly influenced by the term d^m. However, d can only be high, if the source term in eq. (7) is significant relative to the sink term, which means a sufficiently high a/b ratio.

Another important effect is the temperature dependence of our rheology. In the viscosity law, eq. (6), the temperature dependence is responsible for the higher viscosity of the cold lithosphere. In the damage equation, eq. (7), the temperature dependence of the sink term allows high damage values to occur mostly in the cold lithosphere. In the warmer model mantle the damage heals too fast to produce much viscosity reduction.

3.2 Advection

So far, we have not discussed the time dependence of the damage parameter and the advection term in eq. (7). The advection term, for one, has a destructive effect on the low-viscosity bands. To illustrate

this, we prescribe a special 2-D velocity field, neglect the temperature dependence of the sink term in eq. (7) and in the viscosity law eq. (6) (i.e. $\gamma = 0$) and finally calculate a steady-state solution for the damage parameter from the simplified version of eq. (7) for different values of a and b. Comparing these results will help us to better understand the influence of the advection term in the damage parameter equation.

We therefore employ an arbitrary solenoidal velocity field that more or less models corner flow:

$$\mathbf{u} = \hat{\mathbf{x}}\frac{u_0}{1+\mathrm{e}^{\lambda(x-z)}} - \hat{\mathbf{z}}\frac{u_0}{1+\mathrm{e}^{\lambda(z-x)}} \tag{14}$$

(where u_0 and λ are arbitrary constants) as shown in Fig. 3. The local change in the direction of the flow causes a diagonal high strain rate zone in the box. The material flows obliquely to this high strain rate zone and damage can therefore be advected away from where it is produced. In situations where flow is parallel to a linear damage zone (e.g. transform faults), the advection term in eq. (7) vanishes.

The second picture in Fig. 3 shows horizontal cuts through the viscosity fields for $a = 1.0$, $b = 50\,000$; $a = 0.1$, $b = 5000$ and $a = 0.01$, $b = 500$. On the side of the box where the flow comes in, the viscosity is the same in all cases and no influence of the damage parameter is visible. For high a and b the LVB is quite sharp, deep and nearly symmetric (as expected in the limit of infinite a and b). For decreasing a and b the asymmetry of the LVB increases, in particular the slope of the downstream side decreases, the LVB becomes wider and flatter and the position of the minimum viscosity is advected away from the position of the maximal strain rate. The damage parameter is clearly transported with the material. In our 2-D calculations, we often see situations similar to this later example, in which material movement is oblique to the LVB. So the advection term is always relevant for our 2-D calculations; thus the ratio a/b is not the only determining factor in our results (as in eq. 12), the absolute values of a and b influence the width and depth of the LVBs.

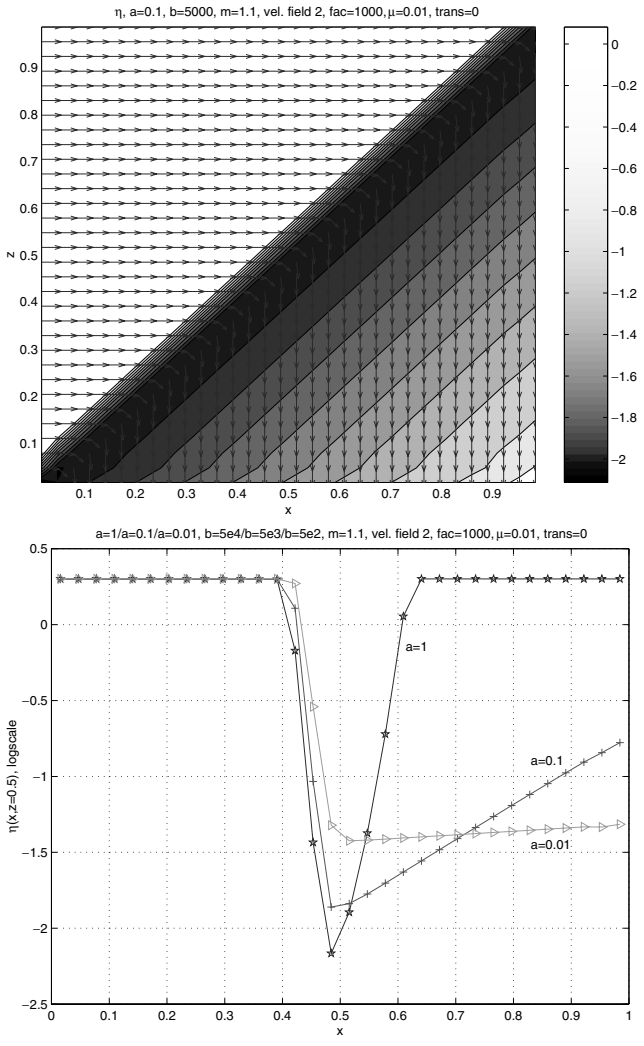

Figure 3. Top: viscosity (grey isolines, $a = 0.1, b = 5 \times 10^4$) and prescribed velocity field (arrows) for investigating the influence of advection in the damage equation. Bottom: horizontal cuts through the viscosity fields for three different sets of a and b. Parameters for the velocity field given in eq. (14) are $u_0 = 1000$ and $\lambda = 100$.

3.3 Influence of damage on velocity: a simple example

In the previous examples we simplified our model by eliminating the coupling between the Stokes equations and the damage parameter equation. Thus we were able to show that self-lubricating behaviour can be expected, and how the advection term in the damage equation, eq. (7), influences the viscosity. The full interaction between velocity and damage is, however, not yet demonstrated; to do this, we must solve the whole set of the governing equations. This is done here for a simple example showing the basics of the evolution of a LVB. We choose our model parameters as follows: $Ra = 10^4$, $\gamma = \ln(10^3)$ (as throughout the paper, but which is really the lower limit of realistic viscosity variability), $a = 0.04$, $b = 10^4$ and $m = 2$. The result will be a steady state with little influence from the advection term. We initiate the calculation with a temperature field obtained from the corresponding isoviscous calculation and $d = 1.0$ everywhere.

Fig. 4 shows the viscosity fields at the beginning of the calculation, after a short time and the final steady-state viscosity. Also presented are the horizontal velocity fields corresponding to the first two viscosities. Finally, the horizontal surface velocity for all cases is shown. It can be seen, that a 'v'-shaped LVB evolves above the downwelling, while the velocity field tends to become a 'corner-flow' similar to that of the second example in the last section. A broader zone of viscosity reduction can also be seen above the upwelling, although it is much less developed than above the downwelling. The surface velocity between these two LVBs tends to become increasingly constant and plate-like. As we will see later, this example is quite typical. Although the shape, sharpness and depth of the low-viscosity zones depend on the values of m and a (with a/b constant) and the asymmetry of the system depends on a/b (with b constant), these general plate-like features remain visible in all calculations with significant damage.

4 NUMERICAL APPROACH AND ANALYSIS METHODS

The continuity and Stokes equations are discretized using a finite-volume method and solved with the multigrid algorithm described in Auth & Harder (1999). The temporal discretizations of the energy and damage equations use a Crank–Nicolson scheme, and for the spatial discretization of the advection term a non-linear method suggested by Koren (1993) is used. A multigrid algorithm combined with an iterative defect correction mechanism is used for the solution of these equations (see Trompert & Hansen 1996). For more detailed information concerning the numerical solutions see Auth (2001).

Our model contains several parameters: the box aspect ratio, the Rayleigh number (Ra), the temperature dependence of the viscosity

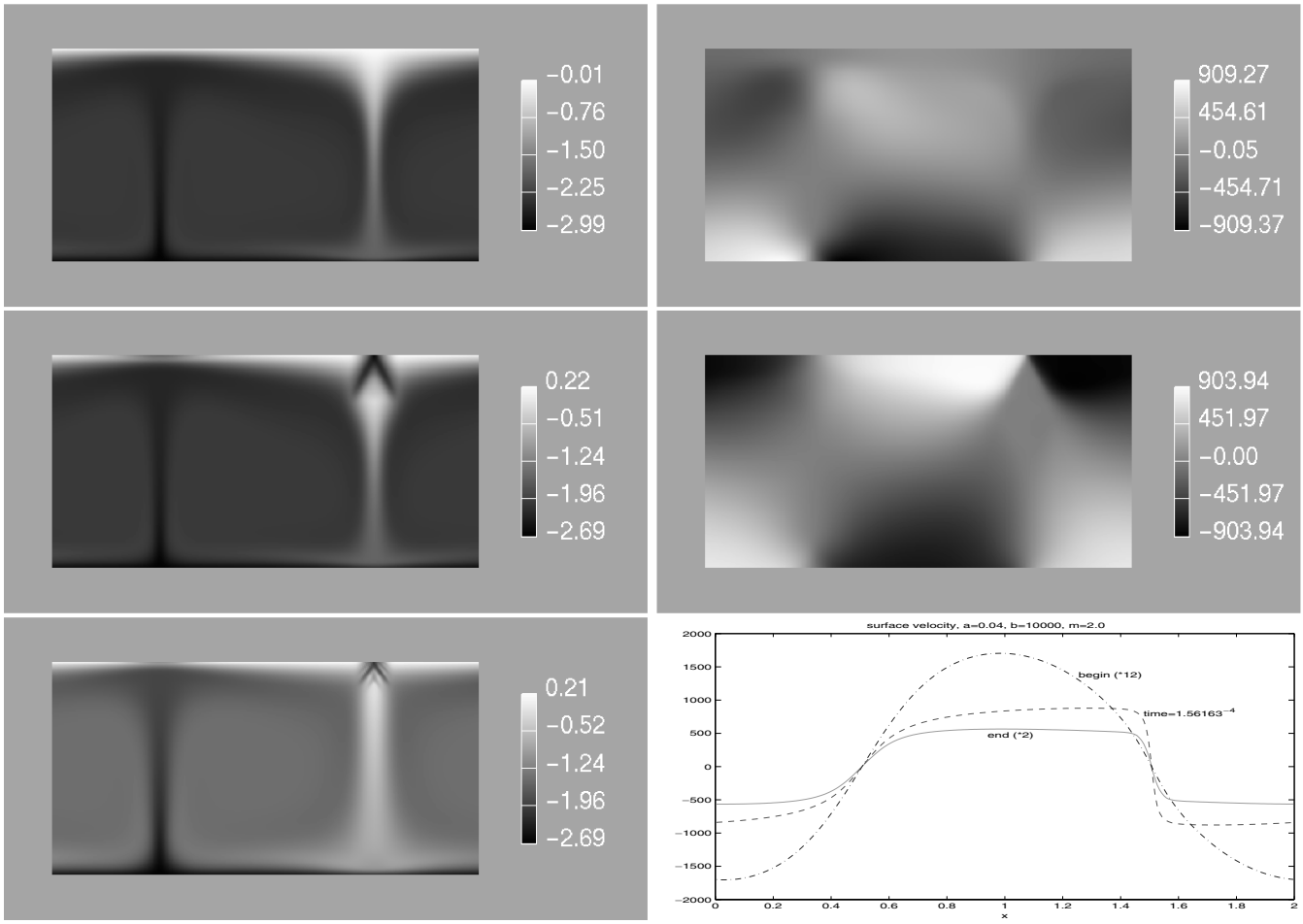

Figure 4. Example for the influence of damage. First row: viscosity and horizontal velocity for a calculation with a pure temperature-dependent viscosity ($Ra = 10^4$, $\gamma = \ln 10^3$). The corresponding temperature field is used as an initial condition for a calculation with damage-dependent rheology ($a = 0.04$, $b = 10^4$, $m = 2.0$, $Ra = 10^4$, $\gamma = \ln 10^3$, $d_{\rm init} \equiv 1.0$). Second row: viscosity and horizontal velocity for the damage-dependent rheology at time $=1.561\,63 \times 10^{-4}$. Third row left: steady-state viscosity field for the damage-dependent rheology. Right: surface velocity corresponding to the three viscosity fields.

and of the healing term in the damage equation (γ), the exponent of the damage parameter in the viscosity law (m) and the magnitude of the damage source and sink terms (a and b). To reduce the number of parameters, we fix the aspect ratio to 2 : 1, $\gamma = \ln \quad (10^3)$ and $Ra = 10^4$. The Rayleigh number is scaled with the surface viscosity $\eta_0(T = 0, d = 1)$; a viscosity scale given by η at a typical mantle temperature of 1500 °C (or 0.5 in non-dimensional quantities), as done by several other authors, would result in an effective Rayleigh number of around 3×10^5. An overview of our calculations is given in Tables 1 and 2. All simulations are extended long enough to become independent of their initial conditions ($T_{\rm init}$ and $d_{\rm init}$). Some of our results will contain very localized low-viscosity bands. From resolution tests we know that the results become independent of resolution if at least five gridpoints sample each LVB in each spatial direction. The results presented here fulfil this criterion, unless stated explicitly otherwise. A cut-off of the viscosity field is never performed. Our principal goal, as described in the introduction, is to improve the 'plate-like behaviour' in free mantle convection simulations. Aspects of plate tectonics on the Earth's surface include homogeneous plate velocities, focused deformation, asymmetric subduction and strike-slip faults. Thus an assessment of our (2-D) calculations according to the following questions is warranted: do we see localized LVBs? Do we see a surface moving with uniform velocity in large areas? Do we see symmetry breaking in subduction behaviour? To measure the homogeneity of the surface velocity during the calculation, we plot the relative number of 'plate points' over time. We define a gridpoint on the surface to be a plate point, if the derivative of its horizontal velocity is at least a thousand times smaller than the maximum derivative of the horizontal surface velocity. The asymmetry of subduction during a calculation can be measured by plotting the horizontally averaged horizontal velocity at a particular depth versus time. Since the horizontal velocity averaged over the whole domain is designed to vanish (given periodic boundary conditions) the line-averaged horizontal velocity should always be zero for a perfectly symmetric convection pattern. We will use the velocity averages at depth $z = 0.25$ and 0.75.

5 BASIC RESULTS

The goal of the following part of this paper is to present the changes in the convection pattern and the plate-like behaviour in our simulations due to variations of single input parameters. This is done in four series, varying a (series A), a and b simultaneously (series AB), and finally varying m (two series, M0 and M1). The quality of the plate-like behaviour is judged in terms of focused LVBs, solid-body-like homogeneous surface velocities and subduction-like symmetry breaking in downwellings. An overview of these calculations is given in Table 1. We refer to the different calculations (or

Table 1. Summary of cases discussed in Section 5.

Series	Case no	a	b	m	Regime
A0	1	0.033	5×10^4	1.1	I
	2	0.10	5×10^4	1.1	II
	3	1.00	5×10^4	1.1	IIIa
	4	5.00	5×10^4	1.1	IIIa
	5	10.0	5×10^4	1.1	IV
AB	1	0.01	5×10^2	1.1	IIIa
	2	0.10	5×10^3	1.1	IIIa
	3	1.00	5×10^4	1.1	IIIa
	4	10.0	5×10^5	1.1	IIIa
	5	20.0	1×10^6	1.1	IV
M0	1	1.00	5×10^4	0.7	IIIa
	2	1.00	5×10^4	1.1	IIIa
	3	1.00	5×10^4	1.3	IIIa
	4	1.00	5×10^4	1.4	IIIb
	5	1.00	5×10^4	1.5	IIIb
	6	1.00	5×10^4	2.0	IIIb
M1	1	0.04	2×10^3	1.1	IIIa
	2	0.04	2×10^3	2.0	IIIa
	3	0.04	2×10^3	3.0	IIIb
	4	0.04	2×10^3	4.0	IIIb

Note that the same parameter combinations can have more than one case number, depending on the series in which it is included (e.g. case A0-3 is identical to case AB-3 and case M0-2).

Table 2. Summary of cases discussed in Section 6.

Series	Case no	a	b	m	Regime
A1	1	0.04	2×10^3	2.0	IIIa
	2	0.08	2×10^3	2.0	IIIa
	3	0.12	2×10^3	2.0	IV
	4	0.16	2×10^3	2.0	IV
	5	0.20	2×10^3	2.0	IV
A2	1	0.008	1×10^4	2.0	I
	2	0.016	1×10^4	2.0	II
	3	0.04	1×10^4	2.0	IIIb
	4	0.20	1×10^4	2.0	IIIb
	5	0.40	1×10^4	2.0	IIIb
	6	0.50	1×10^4	2.0	IV
A3	1	1.00	5×10^4	1.5	IIIb
	2	4.00	5×10^4	1.5	IIIb
	3	5.00	5×10^4	1.5	IV

cases) in the following way: 'name of the series the case belongs to'-'case number in this series'. For example 'A1-2' is the second case in series A1. The same case can have different names if it is included in different series. For example, the labels A0-3, AB-3 and M0-2 all refer to the same case.

5.1 Variation of a, series A0

In the first series of numerical experiments (A0), the influence of the damage source term parameter a shall be tested. We fix the healing term parameter to $b = 5 \times 10^4$ and the exponent of the damage parameter in the viscosity law eq. (6) to $m = 1.1$, which is greater than unity to allow self-lubricating behaviour (see the analysis in Section 3). The parameter b is chosen such that the damage parameter d in material moving with a non-dimensional velocity of 1000 (corresponding to around 1 cm yr^{-1}) would decay to d/e within a distance equal to 1/50th of the length of the box (assuming no source terms for d). For the size of the parameter a we follow the results of Tackley (1998), who used a rheology similar to the asymptotic one in eq. (11), and found an a/b ratio of 10^{-5} to be adequate for producing LVBs. Here we present results for $a = 0.1$, 1.0 and 10.0. For $a \approx 0.033$ the source term in eq. (7) is too small to allow d to become significant and the system tends to a steady state with only temperature-dependent viscosity and no plate-like behaviour.

For $a = 0.1$ we observe episodic behaviour. For long periods convective flow shows very weak upwellings or downwellings, cold

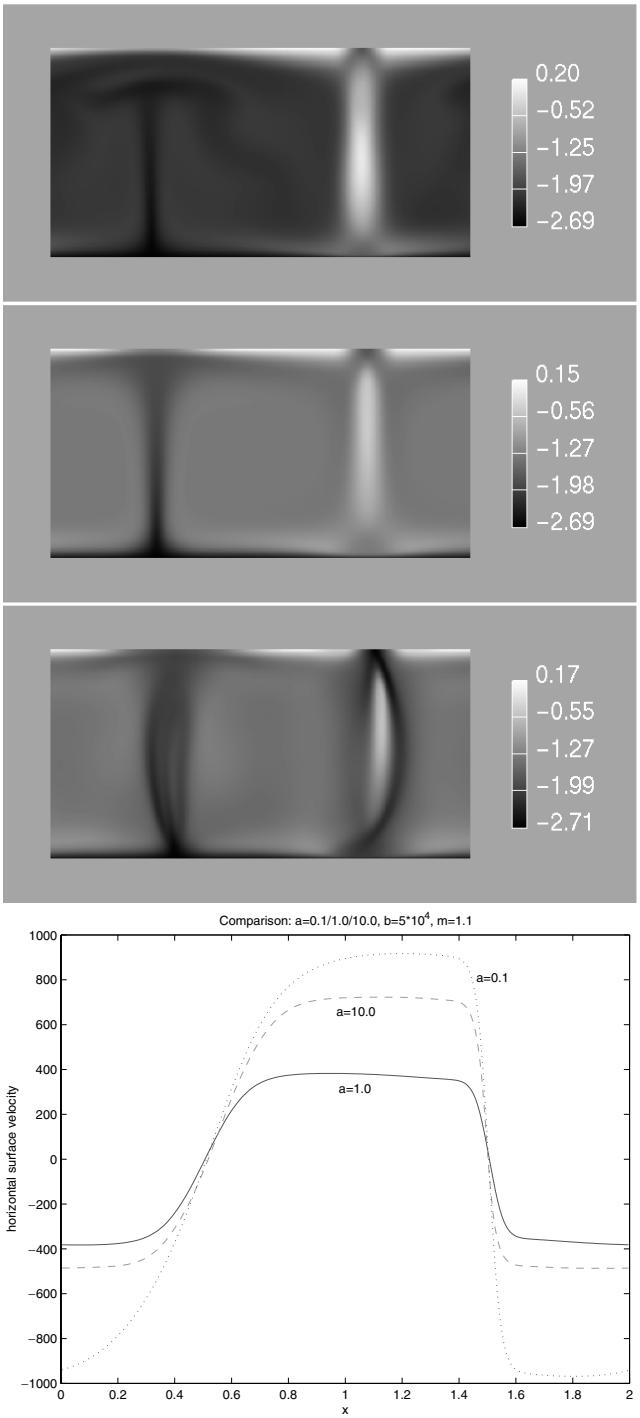

Figure 5. Series A0. From top to bottom: viscosities for cases A0-2 ($a = 0.1$), A0-3 ($a = 1.0$) and A0-5 ($a = 10.0$). Constant parameters: $b = 5 \times 10^4$, $m = 1.1$. Last picture: surface velocity for the three cases.

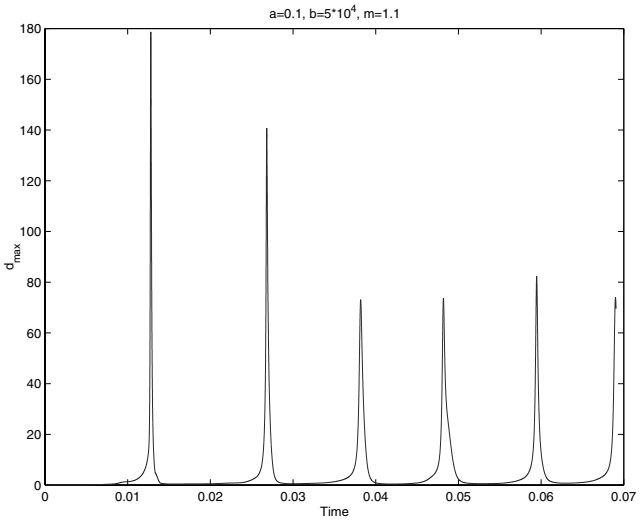

Figure 6. Maximum damage versus time for case A0-2 ($a = 0.1$, $b = 5 \times 10^4$, $m = 1.1$).

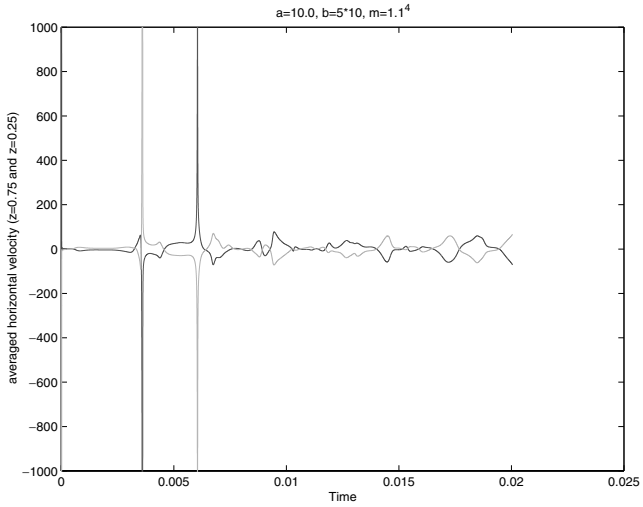

Figure 7. Velocity in the x-direction horizontally averaged for depths $z = 0.25$ and 0.75 versus time for case A0-5 ($a = 10.0$, $b = 5 \times 10^4$, $m = 1.1$).

material is accumulated in the upper thermal boundary layer and the damage is negligible. When the unstable density stratification collapses, fast upwellings and downwellings are produced, accompanied by a strong increase in the damage parameter (Figs 5 and 6). A tendency toward plate-like behaviour is only obtained during periods of fast subduction. We find little asymmetry in the upwellings and downwellings, but the surface velocity of the material clearly differs from a sinusoid, i.e. it hardly varies in regions between the upwelling and downwelling, but it changes very rapidly above the downwelling. The change above the upwelling is less abrupt.

The case $a = 1.0$ produces a steady state with constant influence of the damage parameter; Fig. 5 clearly shows the viscosity reduction above the downwelling for this case. A sharp change in the surface velocity above the downwelling is obtained and a slightly broader change above the upwelling. Between these zones the velocity hardly varies. However, essentially no asymmetry can be found in upwelling or downwelling.

Although we obtain time-dependent behaviour for $a = 10.0$, general features of the convection pattern are stable: the influence of the damage parameter remains significant in large parts of the box. Above the upwelling a broad reduction of viscosity can be seen and the LVB in the downwelling region is more extensive than for $a = 1.0$ and covers the downwelling like a lens. Fig. 5 shows that in this case both the upwelling and downwelling have an asymmetric structure. The convection in the cell in the middle of the box is much more vigorous than in the adjacent cell (see the surface velocity) and the averaged horizontal velocities at depth $z = 0.25$ and 0.75 plotted in Fig. 7 demonstrate that this behaviour oscillates in time. Since the lithosphere is weakened over a broad zone above the upwelling the surface velocity change above the upwelling becomes broader than, for example, in the case $a = 1.0$. Nevertheless, the surface velocity change above the downwelling remains very sharp and the velocity variations between upwelling and downwelling are less gradual than for smaller a.

5.2 Simultaneous variation of *a* and *b*, series AB

In a second series of experiments (AB) we focus on the influence of the advection term. Thus we choose $m = 1.1$, $a/b = 2 \times 10^{-5}$ and a and b are varied simultaneously using $a = 0.01$, 0.1, 1, 10, 20. We observe, that the steady-state viscosity fields for the different a and b values differ significantly from each other only above the downwelling (Fig. 8).

For $a = 0.01$ we see an extended LVB inside which the maximum value of the damage parameter d is around 30 and the maximum strain rate is $\dot{\varepsilon}_{\mathrm{calc}} \approx 14\,000$. In the next three cases the extent of the low-viscosity zone is reduced relative to the $a = 0.01$ case and the maximum value for d is increased to approximately 70 ($\dot{\varepsilon}_{\mathrm{calc}} \approx 13500$). The shape of the LVB changes from a linear structure for $a = 0.1$ to a more 'v'-like structure for higher a.

The case $a = 20$ however, is different. It is not only weakly time dependent, but also shows focused LVBs with lower viscosity than are obtained in the other cases. Instead of one extended 'v'-shaped LVB, there are a few smaller weak zones that are parallel to or crossing one another. The maximum value for the damage parameter in the subduction zone increases to around 240 and $\dot{\varepsilon}_{\mathrm{calc}} \approx 63\,000$.

Despite the differences in the LVBs the surface velocity in all cases is nearly identical except that the velocity variation above the downwelling is more inhomogeneous in the last case (AB-5) and occurs in small jumps, forming 'microplates' in between (Fig. 8). No significant asymmetry in the downwelling is visible in any of the cases.

However, two points can be learned from this series: (1) a good quantity to determine the boundary between non-self-lubricating and self-lubricating behaviour is the maximum strain rate ($\dot{\varepsilon}_{\mathrm{calc}}$). It appears to be nearly constant in the non-self-lubricating regime but increases significantly when self-lubricating occurs. (2) Because of the influence of the advection term in the damage equation the strain rate that has to be exceeded before self-lubricating occurs ($\dot{\varepsilon}_{\mathrm{sl}}(a, b, m)$) is much higher than the corresponding strain rate ($\dot{\varepsilon}_{\mathrm{max}}(a/b, m)$) obtained from our analysis without advection. In this series we do not obtain self-lubricating for $\dot{\varepsilon}_{\mathrm{calc}} \approx 14\,000$, although $\dot{\varepsilon}_{\mathrm{max}} \approx 2000$ can be assumed from Fig. 2.

5.3 Variation of *m*, series M0

The last parameter we investigate is the exponent of the damage parameter in the viscosity law, m. For $a = 1.0$ and $b = 5 \times 10^4$ we present the cases $m = 0.7$, 1.1, 1.3, 1.4, 1.5, 2.0 in Fig. 9. For $m = 0.7$ and 1.1 we obtain a steady-state solution with broad

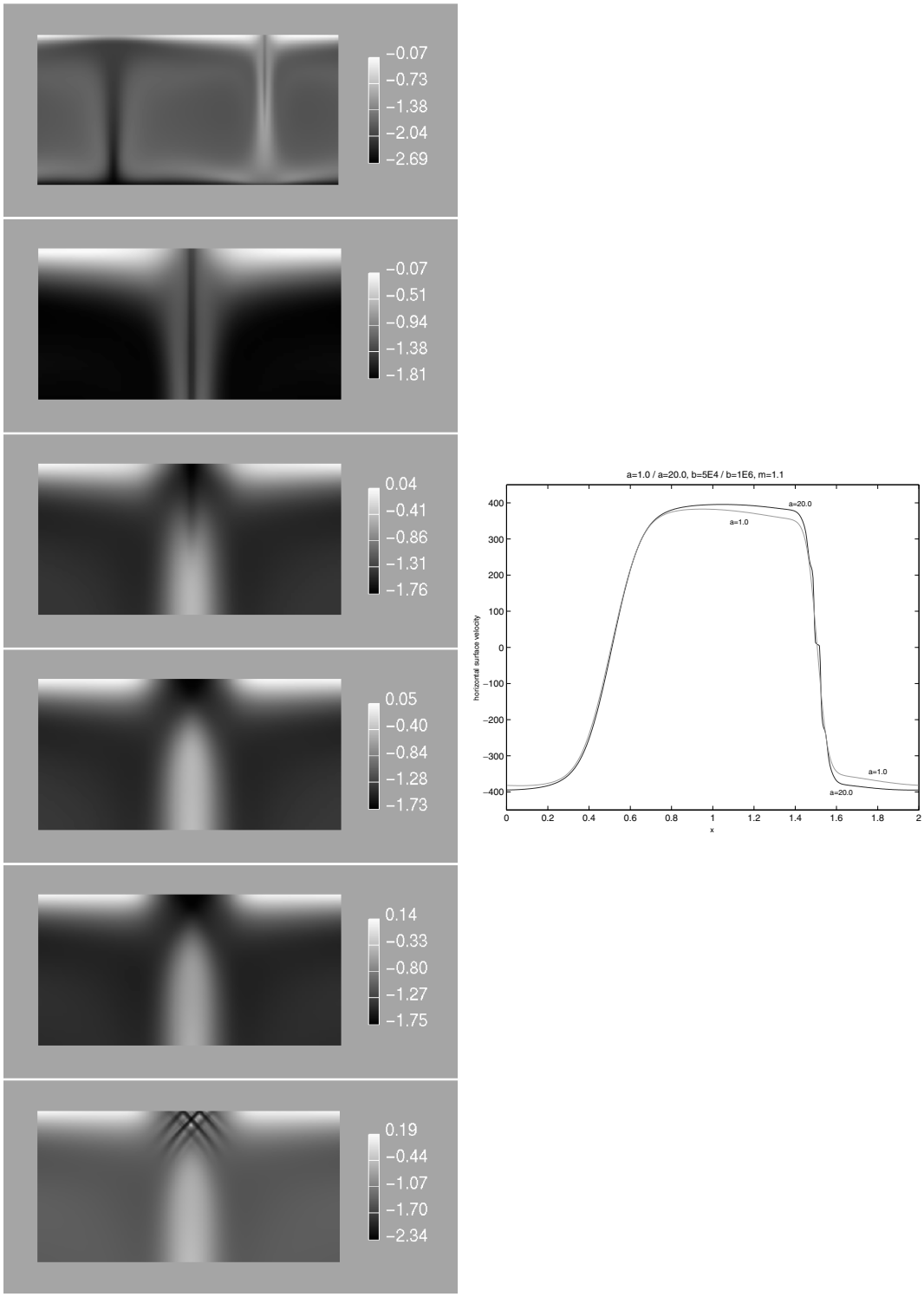

Figure 8. Left-hand column: viscosities for series AB. From top to bottom: case AB-1 ($a = 0.01$, $b = 5 \times 10^2$), downwellings for cases AB-1 ($a = 0.01$, $b = 5 \times 10^2$), AB-2 ($a = 0.1$, $b = 5 \times 10^3$), AB-3 ($a = 1.0$, $b = 5 \times 10^4$), AB-4 ($a = 10.0$, $b = 5 \times 10^5$), and AB-5 ($a = 20.0$, $b = 1 \times 10^6$), constant parameter: $m = 1.1$. Right-hand column: surface velocity for cases AB-3 and AB-5.

LVBs above and below the downwelling and $\dot{\varepsilon}_{\text{calc}} \approx 13\,500$. Case M0-3 ($m = 1.3$) has a weak periodic time dependence but similar LVBs and $\dot{\varepsilon}_{\text{calc}} \approx 14\,200$. For case M0-4 ($m = 1.4$) we see first indications for self-lubricating behaviour: the broad LVBs at the downwelling begin to focus to a few connected narrow LVBs with significant lower viscosity than for case M0-3. A similar process starts above the upwelling, although this is hardly visible in Fig. 9. The maximum strain rate reaches values up to $\dot{\varepsilon}_{\text{calc}} \approx 24\,500$. For a further increase in m the LVBs continue to focus, their viscosity further decreases and $\dot{\varepsilon}_{\text{calc}} \approx 55\,000$ for $m = 1.5$ and $\dot{\varepsilon}_{\text{calc}} \approx 315\,000$ for $m = 2.0$ are obtained. From the magnified parts of case M0-6 ($m = 2.0$) two interesting features can be seen. (1) All LVBs for

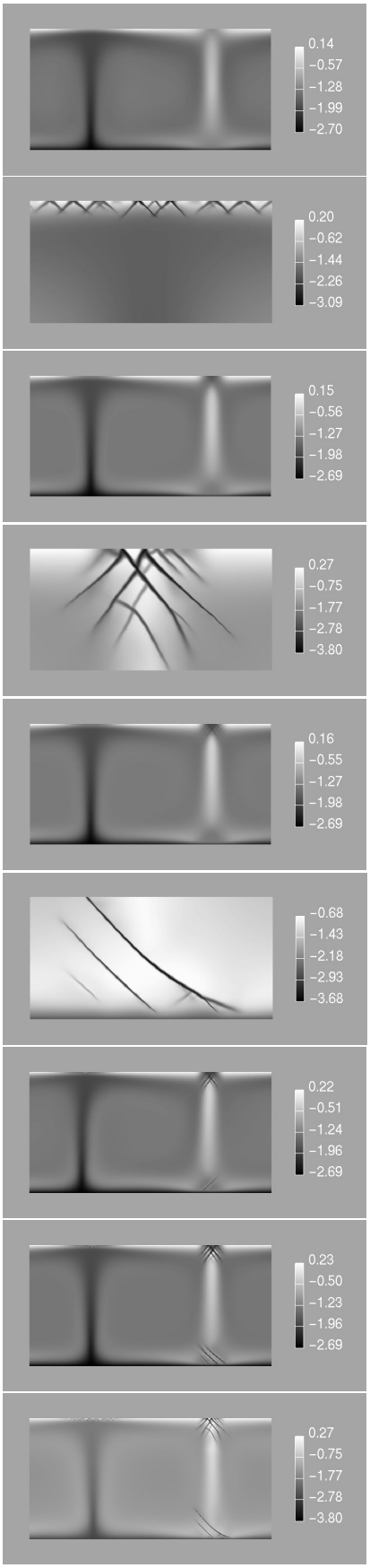

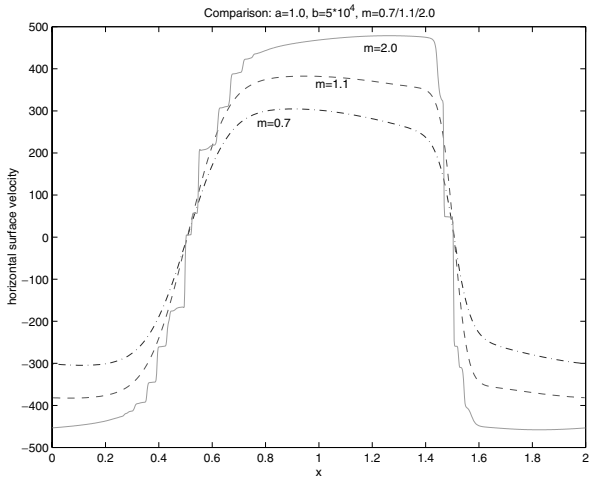

Figure 9. Viscosities for series M0. Left-hand column from top to bottom: cases with $m = 0.7, 1.1, 1.3, 1.4, 1.5, 2.0$, constant parameters: $a = 1.0$, $b = 5 \times 10^4$. Right-hand column: top of the upwelling, top and bottom of the downwelling for $m = 2.0$, surface velocities for $m = 0.7, 1.1, 2.0$.

$m < 2.0$ are orientated in an angle of 45° to the surface. However, for $m = 2.0$ a few LVBs in the downwelling also show angles around 60°. (2) The LVBs at the bottom of the downwelling are asymmetric for all calculations with $m > 1.3$. This asymmetry is a stable feature, although the orientation of the asymmetry can change in time. However, we do not want to overinterpret the case M0-6, because parts of the narrowest LVBs are resolved by fewer than five grid-points.

The focusing of the LVBs above the upwelling and downwelling leads to more discontinuous variations in the surface velocity and the development of microplates. Although the cases with $m > 1.3$ are time dependent the periods of asymmetry are short and this asymmetry is not well developed.

The result that the transition between simulations without and with self-focusing LVBs occurs at $m \approx 1.4$ is somewhat unexpected. From our previous analysis (see eq. 10) one might think, that this transition occurs at $m = 1.0$, since this is the value, where this analysis predicts a change in the material behaviour and since $\dot{\varepsilon}_{\mathrm{calc}} \approx 13\,500$ is high enough to allow this change (see Fig. 2). However, we have seen in the previous section that the absolute values of a and b are not high enough to produce self-focusing behaviour at $m = 1.1$. So why does the transition to self-focusing behaviour happen at higher m? Although the advection term in our simple analysis is neglected (Section 3.1), the general dependence of $\dot{\varepsilon}_{\mathrm{max}}(m)$ (e.g. eq. 12) seems to be correct: $\dot{\varepsilon}_{\mathrm{sl}}$ decreases with increasing m. So self-focusing cannot occur at $m = 1.1$, because the advection of damage is too strong, but it can occur at $m = 1.4$. In short, self-focusing occurs at higher than expected m to adjust for the influence of advection.

5.4 Variation of *m*, series M1

In series M0 the values of a and b are quite high. Thus the influence of advection in the damage equation is low and the structures of the LVBs above the upwelling and downwelling are more 'v'-like than linear, even for small m. Of course increasing m produces self-focusing of the LVBs, but their general 'v' shape is not changed.

In our second series M1 we will show that for lower values of a and b an increase of m is still able to change the structure of the LVBs from more linear to more 'v'-shaped. We now choose $a = 0.04$ and

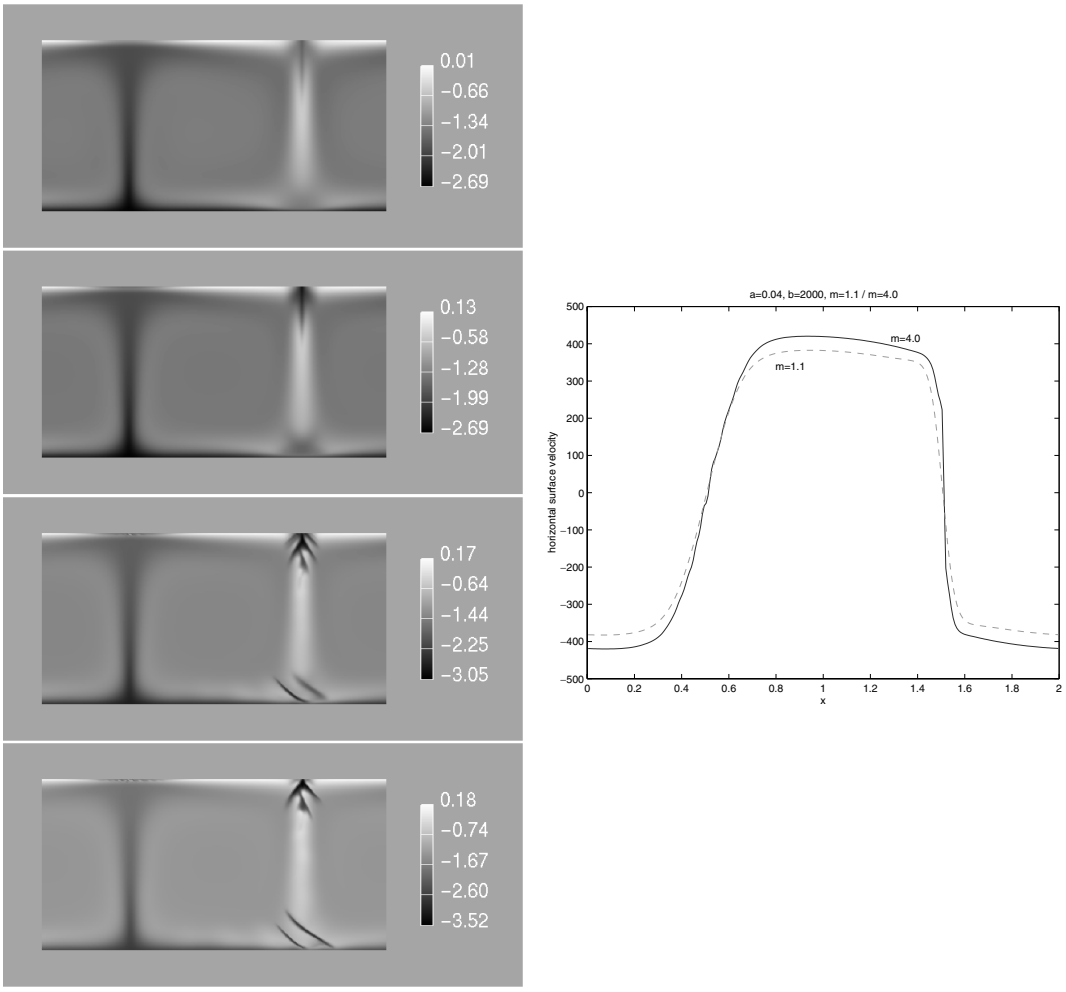

Figure 10. Viscosities and surface velocities for series M1. Left-hand column, from top to bottom: cases M1-1 ($m = 1.1$), M1-2 ($m = 2.0$), M1-3 ($m = 3.0$), M1-4 ($m = 4.0$). Right-hand column: surface velocities for cases M1-1 and M1-4. Constant parameters: $a = 0.04$ and $b = 1 \times 10^3$

$b = 2000$. The results for $m = 1.1$, 2.0, 3.0, 4.0 show significant changes in the viscosity field (Fig. 10).

For $m = 1.1$ and 2.0 the LVBs above the downwelling are linear and we have a horizontally extended LVB above the upwelling; however, there are no LVBs on the bottom of the box.

The cases with $m = 3.0$ and 4.0 in contrast show 'v'-shaped LVBs above the downwelling, an additional LVB beneath it and indications of a focused LVB above the upwelling. Even so the influence of the small a and b values remain visible. The 'v'-shaped LVBs above the downwelling are arranged one beneath the other, while they are side by side and connected for large a and b values. To explain this change in the convection pattern with increased m we note that m is not only included in the viscosity law, but also in the source term of the damage equation, eq. (7), which appears as $a\frac{2}{1+d^m}\mathrm{e}^{-\gamma T}\dot{\varepsilon}^2$. If a calculation is initiated with a linear damage structure (like that for $m = 1.1$, for example) the positions for the maximum d and the maximum $\dot{\varepsilon}$ values are not identical, since d is maximum close to the middle of the subduction zone and $\dot{\varepsilon}$ is maximum where the velocity changes most abruptly. Thus the damage parameter d will increase much more in the regions of high $\dot{\varepsilon}$ than in the regions of already high d. This effect obviously becomes stronger, as m increases. So an increase in m acts against advection and tends to pin the high damage zones to the high strain-rate zones. For each m value, a balance is reached between pure linear structures (influenced primarily by advection) and pure 'v' structures (influenced by strain rate). Even in the more linear structure for $m = 2.0$ a 'v' pattern is visible, and even for 4.0 the 'v' structures are arranged one beneath another.

As with our results in varying a and b simultaneously, the changes in the 'plate-like' behaviour of the system are not significant. The surface velocity is similar for all cases and no microplates occur. Although $m = 3.0$ and 4.0 produce time-dependent behaviour the asymmetry in the subduction zone is negligible.

5.5 Summary of the parameter variations

The increase of a with fixed b and m improves the asymmetry of the system, but values that are too high can weaken large parts of the lithosphere, thereby reducing the areas of plate-like homogeneous surface velocities. The absolute values of a and b, for a/b and m constant, influence the shape of the LVBs above the upwelling or downwelling material. 'Lower' values of a lead to linear structures and 'higher' values to 'v' structures. Temporary asymmetry and very focused LVBs are obtained, when the system enters the self-lubrication regime. What is meant by 'lower' and 'higher' values of a and b depends on the parameter m; m therefore can be used to control whether a calculation is in the self-lubricating regime and to obtain a suitable focusing of the LVBs.

6 ADVANCED RESULTS

6.1 Motivation

In the last section we discussed how the input parameters of our model influence the structure of convective flow. In this section we will use these results to optimize the plate-like behaviour of our simulations by choosing appropriate parameter values. Unfortunately, many potentially interesting cases cannot be calculated because of numerical difficulties. For high values of a, b and m the LVB are too small and their viscosity is too low to ensure their proper resolution and a sufficient convergence of our numerical algorithm. Thus we have to find a middle course between the optimum plate-like behaviour and our numerical capabilities.

Our new series are mainly motivated by the following two results: (1) for $m > 1.0$ high values of a and b can produce very focused LVBs, but this drastically decreases the convergence of our numerical methods. (2) Asymmetry of subduction improves when a is increased. Therefore, our plan is to consider cases that have a good potential for self-lubrication (sufficiently high m), but are easy to compute (a and b not too high), and then to slowly increase the asymmetry in the convective structure (increase a).

Our first series A1 will start with case A1-1: $a = 0.04$, $b = 2000$ and $m = 2.0$ (identical to case M0-2). Since one of our problems with this series will be the focusing of the LVBs above the upwelling the next series A2 will use higher values for a and b. A further increase of a and b is possible numerically only if m is lowered to $m = 1.5$ (see the discussion of series M0). The start of series A3 is therefore A3-1 (equal to M0-5): $a = 1.0$, $b = 5 \times 10^4$, $m = 1, 5$.

6.2 Series A1

Starting with A1-1 ($a = 0.04$) we present cases A1-1 to A1-5, with $a = 0.04$, 0.08, 0.12, 0.16, 0.20, respectively. The steady state we obtain for $a = 0.04$ in case A1-1 was already shown in Fig. 10 (case M1-2). Case A1-2 ($a = 0.08$) produces a similar steady state and is therefore not presented here.

For case A1-3 ($a = 0.12$) the convective structure of the system changes significantly and episodic behaviour is obtained as shown in Fig. 12. In addition, Fig. 11 presents snapshots from the evolution of the viscosity field between two (temporal) maxima of $d_{\max}$. Figs 12 and 11 eludicate the reason for the episodic behaviour: when only a little material is still subducted, a LVB is present above the

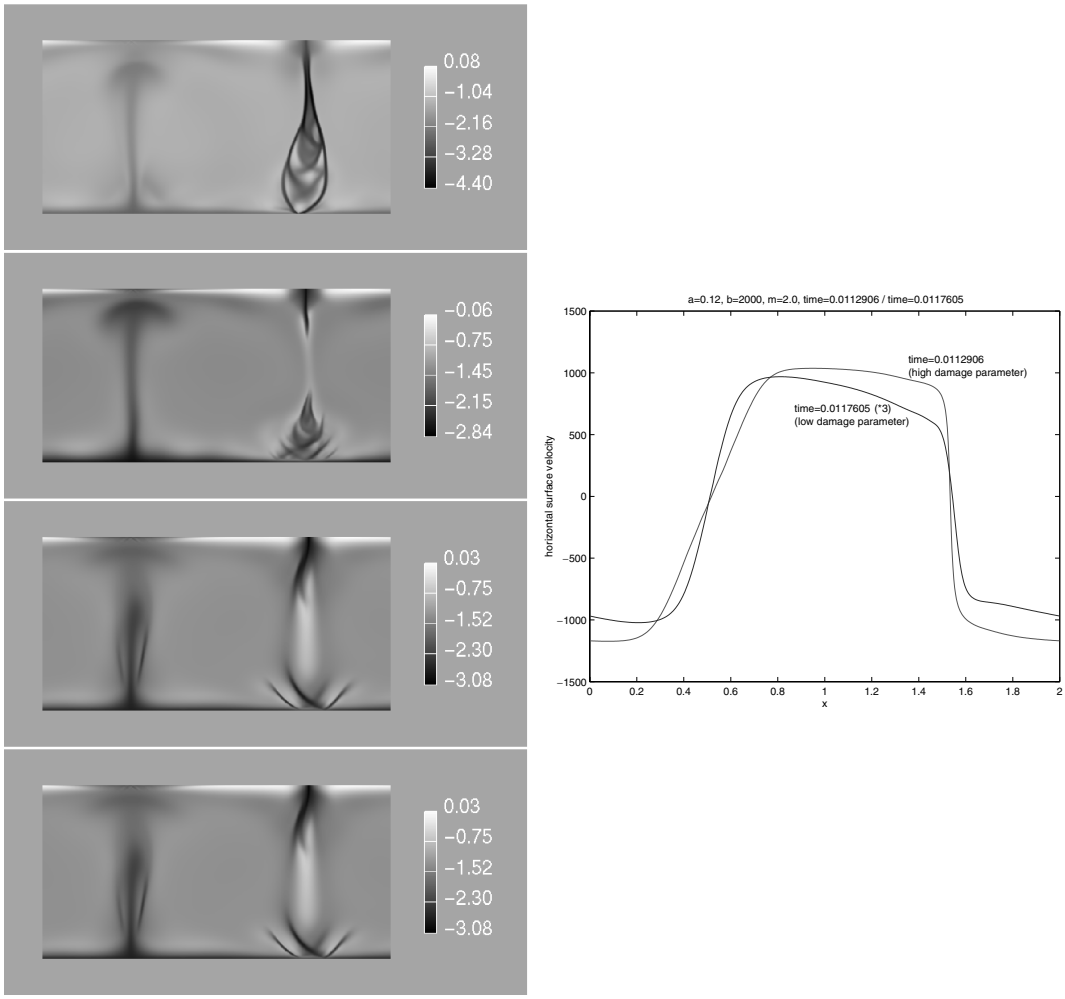

Figure 11. Viscosities and surface velocities for case A1-3 ($a = 0.12$, $b = 2 \times 10^3$, $m = 2$) at different times. Left-hand column: viscosities from top to bottom: at time = 0.009 078 74 and at time = 0.009 263 06 (both at the end of a cycle), at time = 0.011 065 235 and at time = 0.011 249 56 (both at the beginning of the next cycle). Right-hand column: surface velocities at times for which the amount of damage is either large or relatively small, as indicated in the figure.

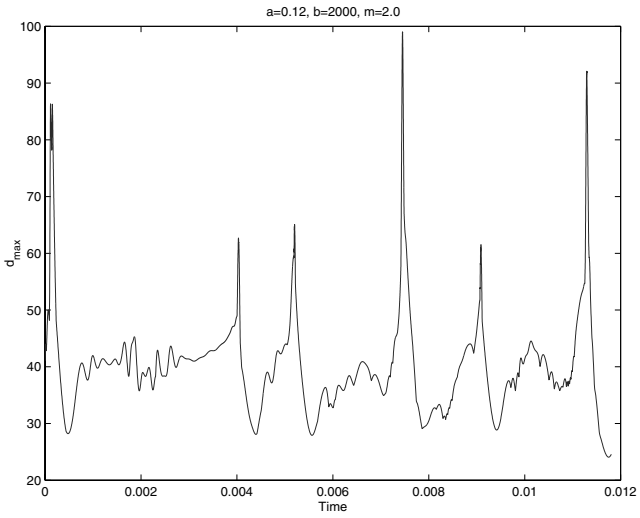

Figure 12. Maximum damage over time for case A1-3 ($a = 0.12$, $b = 2000$, $m = 2$).

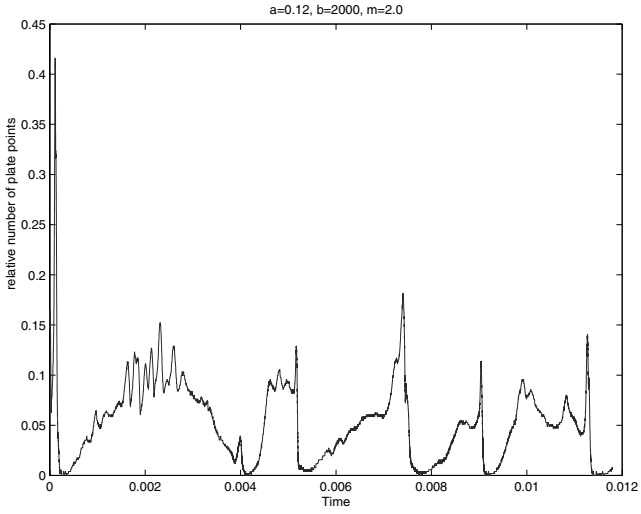

Figure 13. Relative number of plate points for case A1-3 ($a = 0.12$, $b = 2000$, $m = 2$).

subduction zone in the region of high strain rate (see the second picture in Fig. 11). After the first cold subducting material reaches the bottom, LVBs develop there, too, and if the parameter a is high enough, the shear stresses on the sides of the subducting material can be high enough to connect the top and bottom LVB (first, third and fourth pictures in Fig. 11). The coupling between the subducting material and the surrounding material decreases, the subduction becomes faster, causing higher shear stresses on the sides of the subduction zone, the viscosity further decreases, etc. Finally, the subducting material is so fast and the coupling to the material on the top of the box is so weak that the slab breaks (see the second picture in Fig. 11). The rest of the old slab sinks to the bottom of the box, a new subduction starts again on the same position immediately.

How 'plate-like' is the behaviour of the material in this model? Although the LVB above the downwelling has a more linear structure (comparatively low a and b values) the subduction zone is clearly asymmetric (Fig. 11). The plate-like quality of the surface velocity, however, is quite variable. Immediately after the fast subduction of large amounts of cold material into the mantle, the surface material in a large region around the upwelling is hot and has a high damage parameter, so it is quite weak and does not move with homogeneous velocity (Fig. 11). Because of the lower velocity (less slab pull) in the box the region of hot and highly damaged material on the surface diminishes in the following time and the material becomes more rigid in larger parts of the box. When the velocity and the damage parameter start to increase again, those parts subduct with homogeneous velocity and the weak zones above the upwelling grow up again. These variations in the homogeneity of surface velocity can be seen from plotting the relative number of plate points versus time in Fig. 13: we find nearly 15 per cent of the surface gridpoints to be plate points during periods of fast subduction and possibly 1 per cent otherwise. It is significant that this kind of episodic behaviour is completely different from what is observed for case A0-1; in particular, subduction always occurs here, although the velocity of the subducting material is variable. This case is, in fact, more comparable to case A0-3, although convection in A0-3 is less episodic. This is primarily because the viscosity is lower in the LVBs in case A0-3 and these zones are less focused so that the decoupling from the rest of the mantle is less effective. Secondly, the weakening of the slab on the top of the box is less intense in A0-3 than in A1-3.

Although increasing a in A1-1 to A1-3 enhances the asymmetry of subduction, the convective behaviour becomes episodic and the surface velocity inhomogeneous during the periods where there is a broad LVB above the upwelling.

For case A1-4 ($a = 0.16$) we obtain episodic behaviour similar to that for case A1-3 ($a = 0.12$), except it is more extreme. The peaks in the root-mean-square velocity can reach values up to 10^4 (which corresponds to 10 cm yr^{-1} and is around seven times more than the value for A1-3), the maximum damage can come up to 200 (compared with 100 for A1-3), the differences in the vigour of convection in the two different cells increase. It is significant that we see some focusing of the LVBs on the top and on one side of the upwelling at least during some of the episodic events (shown for the fourth event in Fig. 14, although more significant for the second event). Therefore, the surface velocity changes more abruptly above the upwelling than in case A1-3, although the LVB above the upwelling is still extended.

When $a = 0.2$ (case A1-5) the root-mean-square velocity increases to peak values around 2×10^4, and the maximum damage parameter increases to around 240. The differences in the vigour of convection are apparent in Fig. 15. Compared with the fast movement of material in the 'active' cell, the convection in the centre cell is quite weak. Nevertheless, the root-mean-square velocity within the centre cell has approximately the same amount as in cases with much lower a (case A1-1, for example). Corresponding to this situation the asymmetry of the subduction is very high and mostly material from the 'active' cell is subducted. In contrast to cases with lower values of a, a significant asymmetry is also visible in the upwelling. The LVB above the upwelling is much more focused now than in the previous cases. Accordingly the changes in the surface velocity above the upwelling and the downwelling are both very sharp and the velocity through much of the region between them is very homogeneous.

6.3 Series A2

Our major problem in series A1 is the broad LVB above the upwelling. To obtain more focused LVBs the a and b values for our

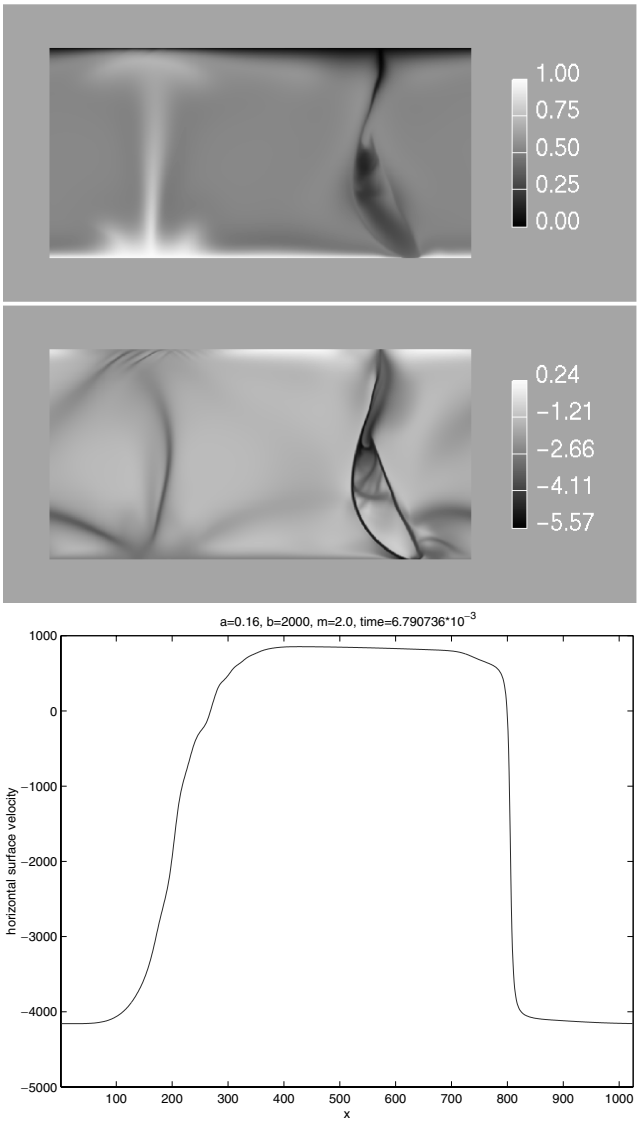

Figure 14. Temperature (top), viscosity (middle) and surface velocity (bottom) for case A1-4 ($a = 0.16$, $b = 2 \times 10^3$, $m = 2$).

new start case A2-4 (cases A2-1/2/3 are not presented in this article) are increased by a factor of 5 compared with case A1-1. A typical viscosity field and the corresponding surface velocity for case A2-4 are shown in Fig. 16. The structure of the LVBs is already very similar to the case M0-6 (a and b increased by another factor of 5; see Fig. 9) except that the zones are broader and the viscosity is not that low, which enables us to perform those calculations with few resolution problems (small parts of the 'v' structure directly above the upwelling are sampled only by three gridpoints).

We now increase a to 0.4 (case A2-5) and 0.5 (case A2-6). A2-5 (not shown here) produces a similar behaviour to A2-4 except that the temporal variation of the damage parameter field is a little higher. For A2-6 we obtain episodic behaviour again; as in case A1-3 we see a sudden increase in the values for the root-mean-square velocity and the damage parameter; moreover, convection is more vigorous in one cell than in the other one and a lens-shaped LVB coats the downwelling (see Fig. 17). A LVB around the upwelling, however, is not visible. Two differences between cases A1-3 and A2-6 are significant: in case A1-3 the LVB on the top of the downwelling is always nearly linear. Also the asymmetry develops a little deeper inside the subduction zone. However, in case A2-6, the subduction asymmetry is clearly visible at the surface, too. The temperature field (Fig. 17) shows subduction with an angle of around 60° to the surface. The second important feature is the LVB above the upwelling. Although this zone becomes broader in case A2-6 compared with case A2-4, the focused 'v'-shaped LVBs survive and the change in the surface velocity is not that homogeneous as it is in case A1-3 (Fig. 17). In fact, the surface velocity changes in a lot of small little jumps and microplates are developed. A further increase of a might be able to improve the plate-like behaviour as in previous examples, unfortunately those calculations are computationally beyond our means.

6.4 Series A3

The parameters a and b can be further increased simultaneously if we decrease m back to $m = 1.5$. Starting from case A3-1 (identical to case M0-5) we first increase a to 4.0 (case A3-2) and then to 5.0 (case A3-3). Case A3-2 gives us a time-dependent but non-episodic result similar to the starting case, the viscosity in the LVBs is lower and the zones are more extended. The result for case A3-3 (Fig. 18) is similar to case A2-6. Therefore, the LVBs above the upwelling can be further focused (compared with case A2-6) and this focusing remains stable during the whole episodic convection. Thus the surface velocity changes in a more plate-like way here, as well.

7 SUMMARY AND DISCUSSION

In this section we summarize and organize our results according to the influence of the different model input parameters, we discuss how plate-like our simulations are and finally we compare our results with other investigations. To remind the reader, the important parameters varied in this study are a, which represents the magnitude of damage caused by deformational work; b controls the loss of damage zones by healing; and m controls the dependence of viscosity on damage (which is necessary for there to be a feedback between the mechanical equations and damage evolution).

7.1 Summary of results

7.1.1 Influence of the parameter a

To facilitate our discussion, we classify our results in terms of parameter a in different regimes. We choose this classification, because the variation of a has the most significant influence on the convective system. For b and m fixed, at least four different regimes of convection can be distinguished; in order of increasing a (relative to a given b) these are as follows.

Regime I. Calculations in this regime show no significant differences with calculations using only a temperature-dependent rheology.

Regime II. In this regime, episodic convection is obtained and damage influences the circulation only during episodes of strong subduction.

Regime III. Convection in this regime either reaches a steady state or is weakly time dependent but with a stable convection pattern. The influence of damage is nearly permanent.

Regime IV. Episodic behaviour ensues again. When a downwelling slab is sufficiently subducted, the entire downwelling is coated in LVBs. This results in very fast downwellings, primarily because the subducting material is decoupled from the rest of the

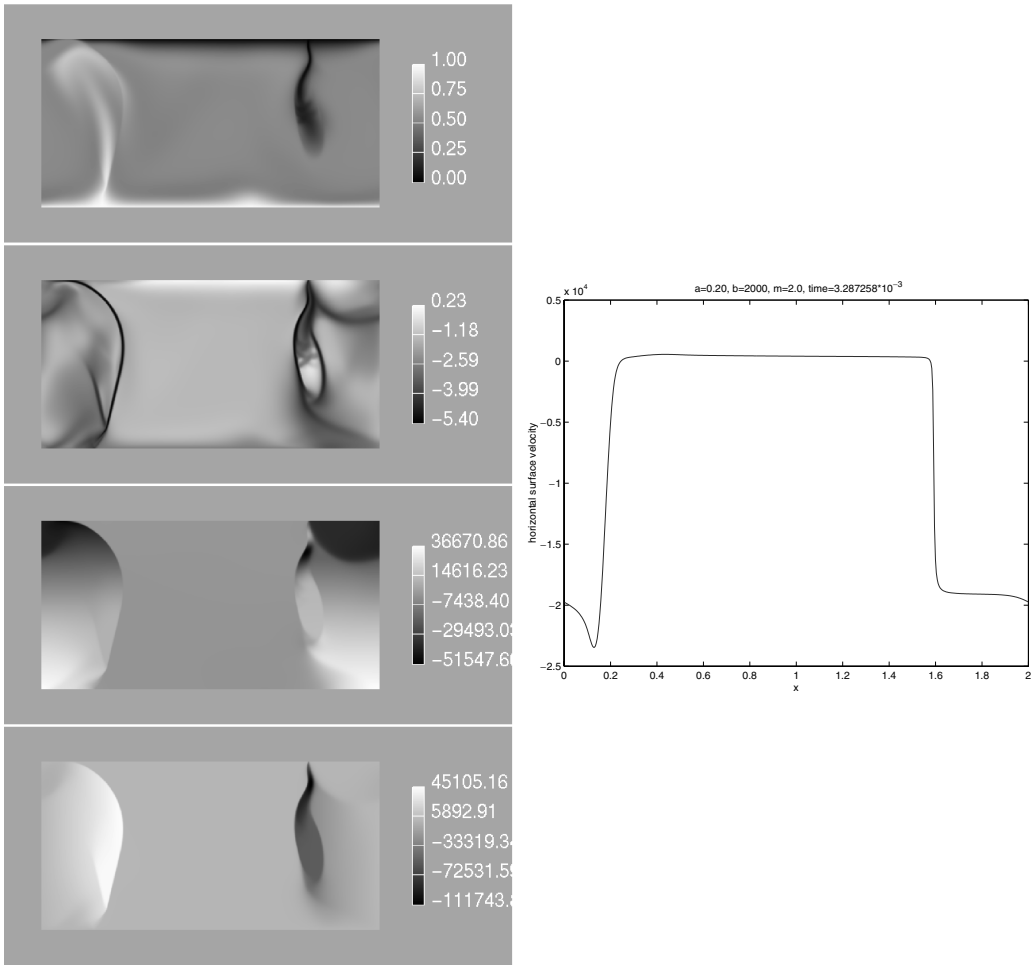

Figure 15. Case A1-5 ($a = 0.2$, $b = 2 \times 10^3$, $m = 2$). Left-hand column, top to bottom: temperature, viscosity, horizontal and vertical velocities. Right-hand column: surface velocity.

mantle. Episodicity itself results from the slab periodically detaching from the upper thermal boundary layer.

An explicit specification of the a values for the boundaries between the different regimes is not presented here, since these values depend on b and m. The computational effort to calculate them for a significant number of b and m would be much too high. However, series A0 and A2 (Tables 1 and 2) might give an idea concerning the boundaries for at least two values of m. Although the b values are different in both series, the results are comparable, since for a fixed value of m the a/b values of the regime boundaries are only weakly variable in the parameter space we investigate here and can therefore be assumed to be constant to a good approximation.

7.1.2 *Influence of advection and the parameter m*

We have shown that the advection of damage significantly influences the convective structures of our system. For cases with low absolute values of a and b (high advection), the LVB are linear; higher values of a and b produce 'v'-shaped LVBs and finally self-focusing of these zones ($m > 1.0$ assumed). Since the transition from non-self-focusing to self-focusing behaviour is very important, we want to include it in our regime classification. The non-self-focusing part of, for example, regime III is therefore called subregime IIIa; the

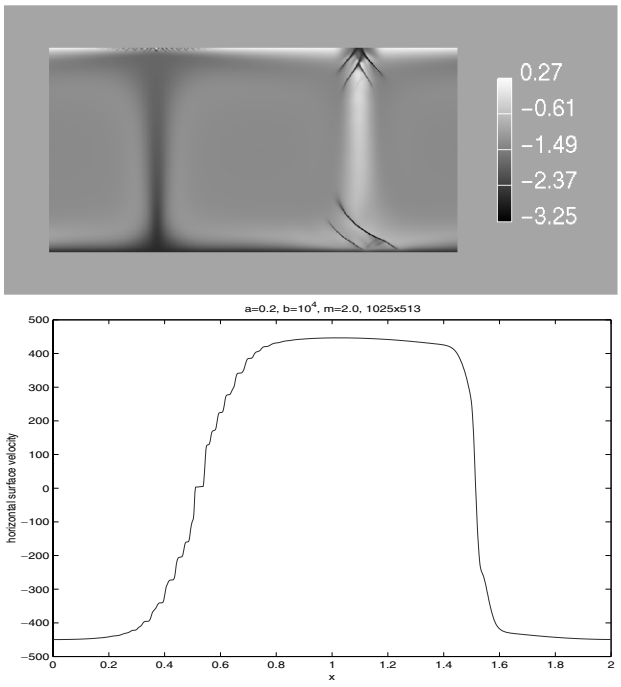

Figure 16. Viscosity (top) and surface velocity (bottom) for case A2-4 ($a = 0.2$, $b = 1 \times 10^4$, $m = 2$).

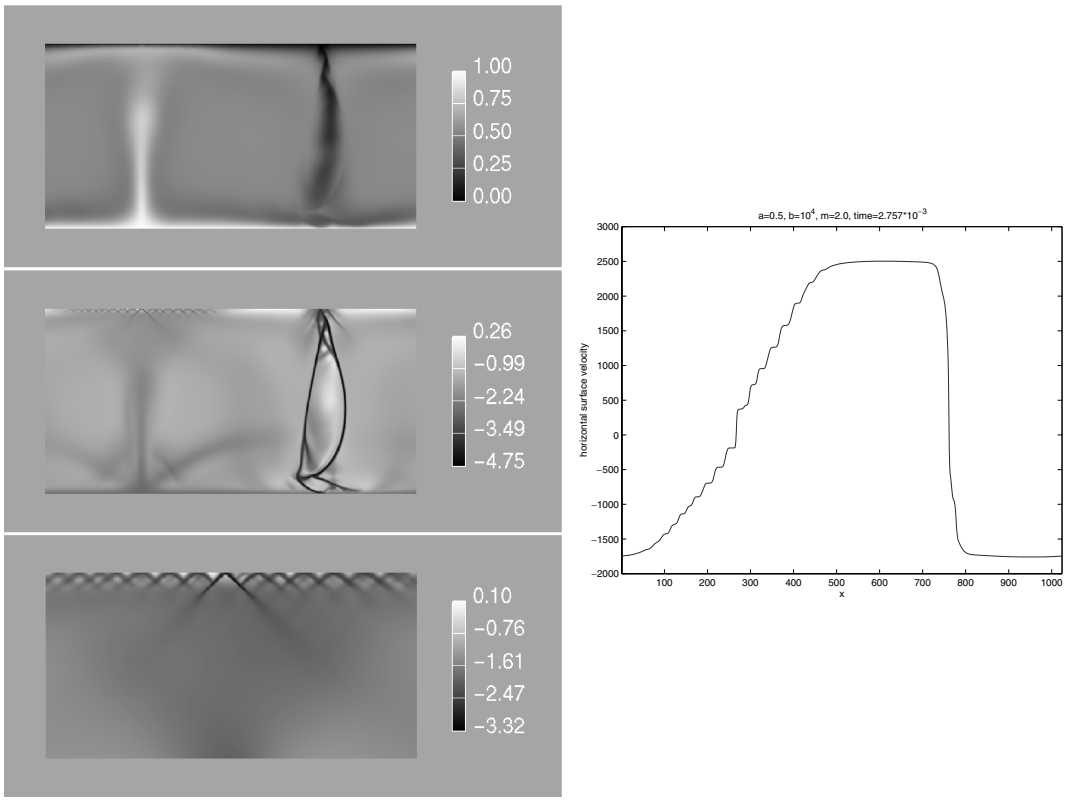

Figure 17. Case A2-6 ($a = 0.5$, $b = 1 \times 10^4$, $m = 2$). Left-hand column, from top to bottom: temperature, full viscosity field and close up of the near-surface viscosity field above the hot upwelling. Right-hand column: surface velocity.

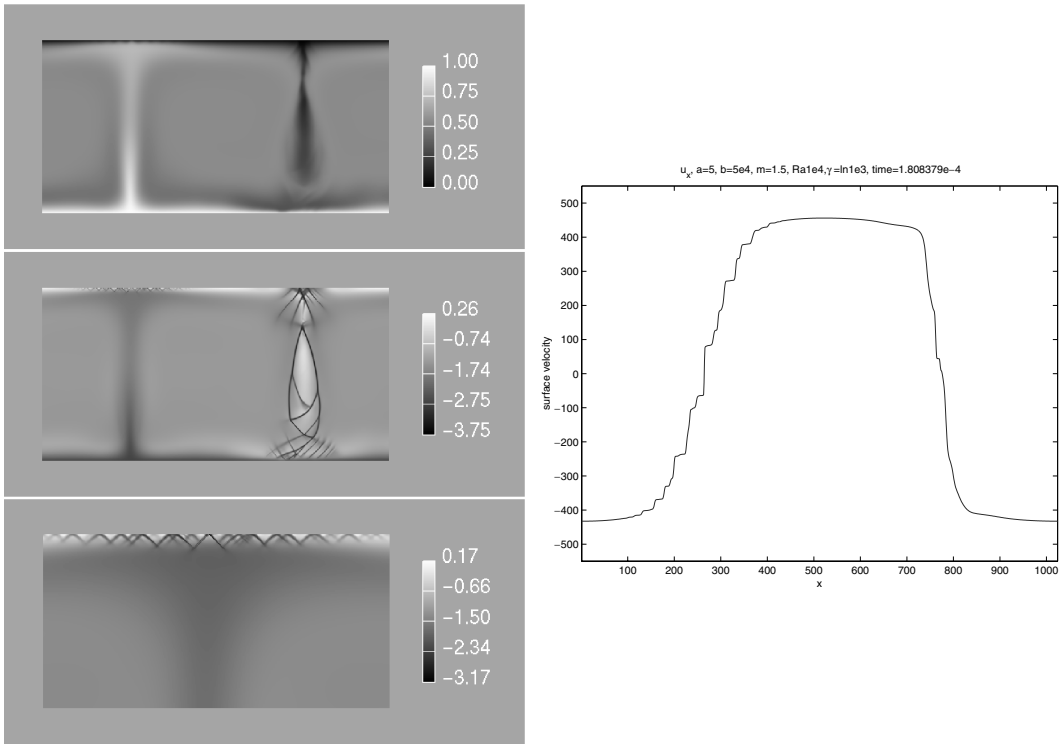

Figure 18. Case A3-3 ($a = 5$, $b = 5 \times 10^4$, $m = 1.5$). Left-hand column, from top to bottom: temperature, full viscosity field and a close up of near-surface viscosity field above the hot upwelling. Right-hand column: surface velocity.

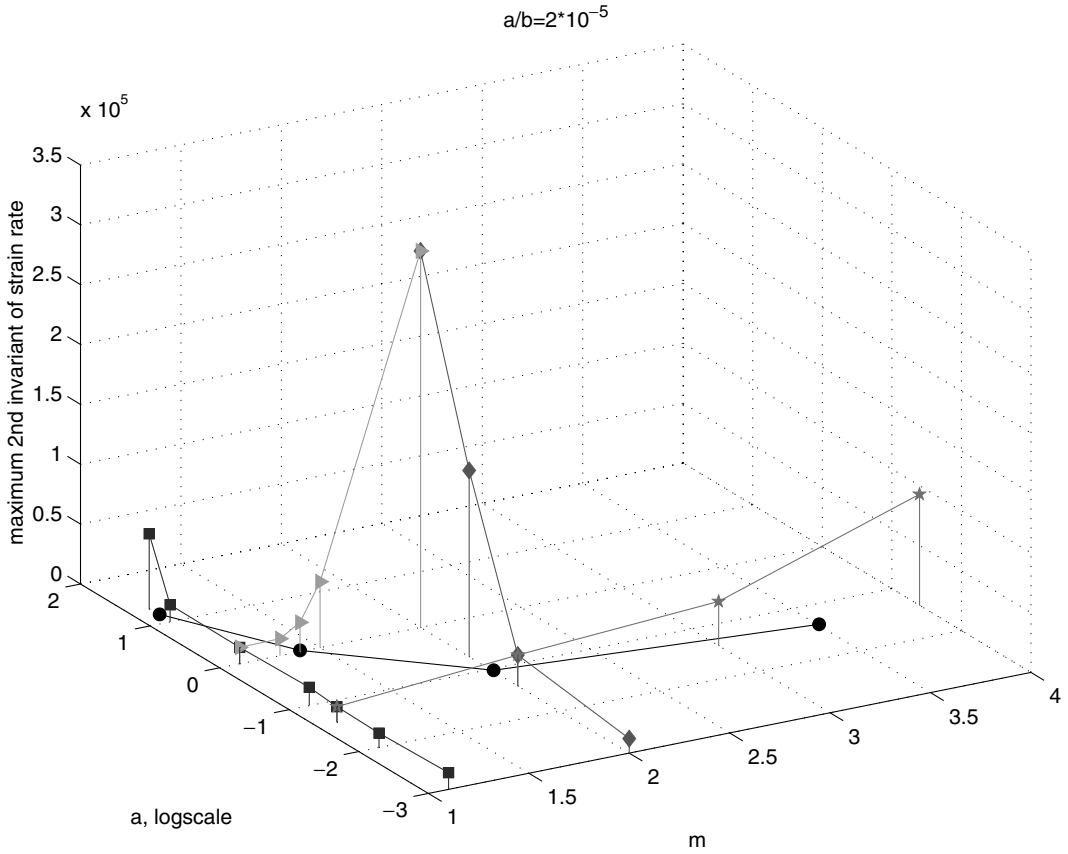

Figure 19. Illustration of the transition between subregimes IIIa and IIIb. Plotted are the time-averaged maximum values of the second strain rate invariant over the *a*–*m* plane, in which the ratio a/b is kept constant at 2×10^{-5}. Points and curves delineated by diamonds, squares, triangles and stars are for calculation series with either increasing a or m that experience a sudden increase in maximum strain-rate. The boundary between the subregimes in the *a*–*m* plane is approximated by the line with solid circles.

self-focusing part is thus subregime IIIb. In fact, regime III is the only regime, in which we observe both non-self-focusing and self-focusing behaviour. Our calculations in regime II always show non-self-focusing behaviour and those in regime IV show self-focusing behaviour.

Following our results in series AB and M0, the boundary between subregimes IIIa and IIIb is determined using the time-averaged maximum of the second invariant of the strain rate tensor $\langle\dot{\varepsilon}\rangle$. Fig. 19 shows $\langle\dot{\varepsilon}\rangle$ over the *a*–*m* plane for a fixed $a/b = 2 \times 10^5$ ratio. The boundary between the subregimes was determined to be where $\langle\dot{\varepsilon}\rangle$ increases suddenly between subregimes (going from IIIa to IIIb). The explanation of the boundary curve between these subregimes was, in fact, already given in our discussion of the influence of the parameter m: an increase in m acts in principle against the advection term in the damage parameter equation (see the section 'Series M1' for further discussion). If a and b are relatively large the advection term in eq. (7) is less important, thus a lower value of m is sufficient to obtain self-focusing behaviour. That the values of $\dot{\varepsilon}$ for the transition between subregimes IIIa and IIIb are much higher than expected from our simple analysis of the damage equation without the advection term (see the section 'Simple analysis without advection') demonstrates the significant influence of the advection of damage for convective structures (see the section 'Series AB' for an extended discussion).

7.1.3 Plate-like behaviour

With an evaluation of our regimes in terms of focused LVBs, homogeneous surface velocities and asymmetric subduction (plate-like behaviour) we arrive at the following results.

(1) Regime I, with the lowest relative a shows no plate-like behaviour at all since little or no damage is present. The surface velocity is nearly sinusoidal, which is thus of low plate-like quality or 'plateness' (Weinstein & Olson 1992).

(2) Regime II shows plate-like tendencies only during episodes of strong subduction. Convection in this regime may be qualitatively comparable to the results of Trompert & Hansen (1998), who observed periods of strong subduction separated by periods with no subduction for calculations with a yield stress rheology.

(3) The LVBs in subregime IIIa are present during the whole calculation, but with elongated and linear shapes. The surface velocity is usually homogeneous, but the transitions over the downwelling and upwelling are quite diffuse. This is comparable to simulations with common power-law rheologies using positive and finite power-law exponents (see, for example, Christensen 1984). Keeping our simple analysis (see eq. 11) in mind, the similarity between damage and power-law rheologies is not surprising, because their $\sigma(\dot{\varepsilon})$ curves are similar before $\dot{\varepsilon}_{\rm sl}$ is reached (see Fig. 1). In subregime IIIb, the LVBs are much more focused than in regime IIIa, and are

more or less 'v'-shaped. Such 'v' structures are also found in studies of localization in compressive folding using power-law rheologies with negative exponent (Montési & Zuber 2002). The surface velocity is much more homogeneous, with a few jumps over the upwelling (microplates) and one or two big jumps over the downwelling. The asymmetry of the subduction is usually not very developed.

(4) The appeal of regime IV is that subduction is usually asymmetric. However, the subduction process is also episodic. This kind of episodicity is not the same as in regime II, because here subduction never really stops, although the slab breaks off from the surface. The differences in the surface velocities therefore occur because of the different pull of the already subducted material on the rest of the lithosphere. During episodes of strong slab pull the surface velocity is usually much too high. A non-dimensional velocity of 1000 in our calculations roughly corresponds to a real velocity of about 1 cm yr^{-1}. So, compared with the velocity of the Earth's plates, non-dimensional velocities much higher than, say, 10^4 are unrealistic. In addition, the LVB above the upwelling can become very diffuse during these episodes of strong slab pull, causing a very unridge-like velocity change right there. This problem mostly occurs for relatively low values for b, when regime IV is entered from subregime IIIa.

7.2 Conclusion

In the end, this study shows that this kind of simple damage rheology can produce very focused LVBs in or above upwellings and downwellings. For high a, b and m values these zones look very much like conjugate shear zones, as observed in different normal and thrust fault geological environments. Despite the very strong limitations in the geometry of our models (e.g. 2-Dity) we have shown that asymmetric subduction can occur using this kind of rheology. The angle of subduction can be changed between 90° (symmetrical subduction) and 45° by modifying the absolute values of a and b compared with the advection term in eq. (7). We have also demonstrated that for appropriate values of the input parameters the surface velocity can be very homogeneous between up- and downwelling, with strongly localized jumps in between.

From a physical perspective, the occurrence of LVBs is associated with a strong feedback mechanism between focusing of deformation on damaged weak zones and the creation of damage by deformational work (see Bercovici & Karato 2003; Regenauer-Lieb & Yuen 2003). The efficiency of this feedback mechanism, and hence the intensity and longevity of the low-viscosity bands, requires that creation of damage by deformational work, and the loss of damage zones by self-healing, must be much more significant than advective loss of damage. If advection is dominant in the damage-evolution equation, it will sweep away damage zones before they have a chance to be sufficiently focused and thus lessen the effectiveness of the intrinsic feedback mechanism.

From those results and results from Bercovici (1996, 1998), who successfully used similar rheology to produce transform faults in a 2-D horizontal layer, we expect that this kind of self-lubrication damage rheologies will produce acceptable plate-like behaviour in 3-D calculations, if sufficiently high values of a and b are used. This expectation stands a little in contrast to work recently done by Tackley (2000b,c) who includes a similar type of rheology in 3-D internally heated calculations. His damage parameter equation is the same as ours, but he adopted a linear viscosity law $\eta_{\mathrm{eff,dam}} = (1 - d)\,\eta_{\mathrm{eff}}$, where η_{eff} is a yield stress viscosity. Keeping a fixed, Tackley presents three calculations with different b and concludes that this kind of rheology: (1) improves localization at spreading centres, but tends to fragment plates and (2) weakens convergent zones and makes downwellings episodic. Both the weakening of convergent zones and the fragmentation of plates could point to too strong an influence of damage advection, possibly in combination with a too strong source term a. However, Tackley's conclusion, that the localization of spreading centres improves with damage rheology, is clearly a point in favour of such rheologies. Nevertheless, the ability of the damage rheology to produce passive spreading in an internally heated system has yet to be shown.

There still remains the problem of episodic behaviour in calculations with significant asymmetry of subduction. As a solution to this problem (see Tackley 2000c; Richards *et al.* 2001) might be the introduction of a low-viscosity asthenosphere, which would reduce the coupling between plates and the mantle, and possibly inhibit the break off of the slab. A similar effect could be obtained with the incorporation of phase transitions and/or the modest viscosity jump at the 660 km discontinuity; either or both of these effects could also inhibit the detachment and loss of slabs from the upper thermal boundary layer.

ACKNOWLEDGMENTS

The authors thank Yanick Ricard, Marc Monnereau and an anonymous reviewer for their thoughtful comments. Support was provided by NSF (grant no EAR-0105269).

REFERENCES

Auth, C., 2001. Plate tectonics in computational simulations of terrestrial mantle convection with grain-size-dependent rheology, *PhD thesis,* Universität Göttingen, Göttingen, Germany, http://webdoc.gwdg.de/diss/2002/auth.

Auth, C. & Harder, H., 1999. Multigrid solution of convection problems with strongly variable viscosity, *Geophys. J. Int.,* **137,** 793–804.

Bercovici, D., 1993. A simple model of plate generation from mantle flow, *Geophys. J. Int.,* **114,** 635–650.

Bercovici, D., 1995. A source-sink model of the generation of plate tectonics from non-Newtonian mantle flow, *J. geophys. Res.,* **100,** 2013–2030.

Bercovici, D., 1996. Plate generation in a simple model of lithosphere–mantle flow with dynamic self-lubrication, *Earth planet. Sci. Lett.,* **144,** 41–51.

Bercovici, D., 1998. Generation of plate tectonics from lithosphere–mantle flow and void-volatile self-lubrication, *Earth planet. Sci. Lett.,* **154,** 139–151.

Bercovici, D., 2003. The generation of plate tectonics from mantle convection, *Earth planet. Sci. Lett.,* **205,** 107–121.

Bercovici, D. & Karato, S., 2003. Theoretical analysis of shear localization in the lithosphere, in, *Reviews in Mineralogy and Geochemistry: Plastic Deformation of Minerals and Rocks,* Vol. 51, Ch. 13, pp. 387–420, eds Karato, S. & Wenk, H., Misn. Soc. Am., Washington, DC.

Bercovici, D. & Ricard, Y., 2003. Energetics of a two-phase model of lithospheric damage, shear localization and plate–boundary formation, *Geophys. J. Int.,* **152,** 1–16.

Bercovici, D., Ricard, Y. & Richards, M., 2000. The relation between mantle dynamics and plate tectonics: a primer, in *History and Dynamics of Global Plate Motions, Geophysics Monograph Series,* Vol. 121, pp. 5–46, eds Richards, M.A., Gordon, R. & van der Hilst, R., Am. Geophys. Union, Washington, DC.

Bercovici, D., Ricard, Y. & Schubert, G., 2001a. A two-phase model of compaction and damage, 1. General theory, *J. geophys. Res.,* **106,** 8887–8906.

Bercovici, D., Ricard, Y. & Schubert, G., 2001b. A two-phase model of compaction and damage, 3. Applications to shear localization and plate boundary formation, *J. geophys. Res.,* **106,** 8925–8940.

Braun, J., Chery, J., Poliakov, A., Mainprice, D., Vauchez, A., Tomassi, A. & Daignieres, M., 1999. A simple parameterization of strain localization in the ductile regime due to grain size reduction: a case study for olivine, *J. geophys. Res.,* **104,** 25 167–25 181.

Christensen, U., 1984. Convection with pressure- and temperature-dependent non-Newtonian rheology, *Geophys. J. R. astr. Soc.,* **77,** 343–384.

Christensen, U. & Harder, H., 1991. Three-dimensional convection with variable viscosity, *Geophys. J. Int.,* **104,** 213–226.

Gurnis, M., Zhong, S. & Toth, J., 2000. On the competing roles of fault reactivation and brittle failure in generating plate tectonics from mantle convection, in *History and Dynamics of Global Plate Motions, Geophysics Monograph Series,* Vol. 121, pp. 73–94, eds Richards, M.A., Gordon, R. & van der Hilst, R., Am. Geophys. Union, Washington, DC.

Karato, S., 1983. Grain-size distribution and rheology of the upper mantle, *Tectonophysics*, **104,** 155–176.

Koren, B., 1993. Numerical methods for advection–diffusion problems, in *Notes on Numerical Fluid Mechanics,* Vol. 45, ed. Vreugdenhil, C., Vieweg, Braunschweig.

Krajcinovic, D., 1996. *Damage Mechanics,* North-Holland, Amsterdam.

Lemaitre, J., 1992. *A Course on Damage Mechanics,* Springer-Verlag, New York.

Lyakhovsky, V., Ben-Zion, Y. & Agnon, A., 1997. Distributed damage, faulting, and friction, *J. geophys. Res.,* **102,** 27 635–27 649.

Montési, L. & Zuber, M., 2002. A unified description of localization for application to largescale tectonics, *J. geophys. Res.,* **107,** 10.1029/2001JB000465.

Regenauer-Lieb, K. & Yuen, D., 2003. Modeling shear zones in geological and planetary sciences: solid- and fluid- thermal-mechanical approaches, *Earth Sci. Rev.*, in press.

Ricard, Y. & Bercovici, D., 2003. Two-phase damage theory and crustal rock failure: the theoretical 'void' limit, and the prediction of experimental data, *Geophys. J. Int.,* submitted.

Ricard, Y., Bercovici, D. & Schubert, G., 2001. A two-phase model of compaction and damage, 2, Applications to compaction, deformation, and the role of interfacial surface tension, *J. geophys, Res.,* **106,** 8907–8924.

Richards, M., Yang, W.-S., Baumgardner, J. & Bunge, H.-P., 2001. Role of a low-viscosity zone in stabilizing plate tectonics: implications for comparative terrestrial planetology, *Geochem. Geophys. Geosystems (G^3),* **2,** 2000GC000, 115.

Tackley, P., 1998. Self-consistent generation of tectonic plates in three-dimensional mantle convection, *Earth planet. Sci. Lett.,* **157,** 9–22.

Tackley, P., 2000a. The quest for self-consistent generation of plate tectonics in mantle convection models, in *History and Dynamics of Global Plate Motions, Geophysics Monograph Series,* Vol. 121, pp. 47–72, eds Richards, M.A., Gordon, R. & van der Hilst, R., Am. Geophys. Union, Washington, DC.

Tackley, P., 2000b. Self-consistent generation of tectonic plates in time-dependent, three-dimensional mantle convection simulations, 1. Pseudo-plastic yielding, *Geochem. Geophys. Geosystems (G^3)*, **1,** 2000GC000, 036.

Tackley, P., 2000c. Self-consistent generation of tectonic plates in time-dependent, three-dimensional mantle convection simulations, 2. Strain weakening and asthenosphere, *Geochem. Geophys. Geosystems (G^3),* **1,** 2000GC000, 043.

Tackley, P., 2000d. Mantle convection and plate tectonics: toward and integrated physical and chemical theory, *Science,* **288,** 2002–2007.

Trompert, R. & Hansen, U., 1996. The application of a finite volume method to three-dimensional flow problems in a highly viscous fluid with a variable viscosity, *Geophys. astrophys. Fluid Dyn.,* **83,** 261–291.

Trompert, R. & Hansen, U., 1998. Mantle convection simulations with rheologies that generate plate-like behaviour, *Nature,* **395,** 686–689.

Weinstein, S. & Olson, P., 1992. Thermal convection with non-Newtonian plates, *Geophys. J. Int.,* **111,** 515–530.